Working Title:

The cytokine receptor Fn14 regulates neuronal transcription during development and brain function in the adult

Authors:

Austin Ferro, Uma Vrudhula, Yohan S.S. Auguste, and Lucas Cheadle*

*Correspondence: cheadle@cshl.edu

Author affiliations:

Cold Spring Harbor Laboratory, Cold Spring Harbor, NY 11724

Keywords:

Microglia, cytokine, sensory experience, synapse, refinement, synapse elimination, Fn14, TWEAK, memory, hippocampus, dLGN

Summary:

Cytokine signaling between microglia and neurons is required for synapse elimination during brain development, but the mechanisms by which neurons respond to microglia-derived cytokines remain to be fully defined. Here, we demonstrate that microglia are necessary for sensory experience-dependent synapse elimination in the dorsal lateral geniculate nucleus (dLGN) of the mouse, a process previously shown to be mediated by the microglia-derived cytokine TWEAK and its neuronal receptor Fn14. Single-nucleus RNA-sequencing in mice lacking Fn14 or TWEAK at the height of experience-dependent refinement revealed that TWEAK-Fn14 signaling coordinates robust programs of gene expression in excitatory thalamocortical neurons of the dLGN. Gene targets of TWEAK and Fn14 are enriched for regulators of synapse and chromatin remodeling, suggesting that TWEAK-Fn14 signaling coordinates neuronal transcription to promote circuit refinement and epigenomic maturation in response to experience. We further find that Fn14 expression is not restricted to the dLGN but extends to other brain regions as well, both during development and in the adult. Consistent with the expression of Fn14 outside of the visual system, Fn14 knockout mice show significant impairments in multiple tests of memory task proficiency. At baseline, loss of Fn14 does not affect macroscopic neural activity measured by electroencephalogram recordings *in vivo*. However, mice lacking Fn14 displayed worse seizure outcomes and were less likely to survive when seizures were pharmacologically induced. Thus, TWEAK-Fn14 signaling coordinates neuronal transcription during development and contributes to cognitive function in the adult. Taken together, these data reveal that molecular pathways associated with inflammation in the periphery can coordinate with sensory experience to shape neuronal transcription and connectivity across the lifespan.

Highlights:

- Microglia regulate sensory-dependent refinement at the retinogeniculate synapse
- TWEAK-Fn14 signaling induces the expression of neuronal genes involved in synaptic and chromatin remodeling
- Fn14 signaling is dispensable for learning but required for memory in multiple tasks
- Loss of Fn14 exacerbates seizure susceptibility and the severity of seizure outcomes

Introduction:

The precise organization of synaptic connections between defined neuronal partners is the basis of mature brain function. These connections are established in a step-wise fashion, beginning with the formation of an overabundance of synapses and concluding with a refinement process in which a subset of these synapses is strengthened and maintained while others are eliminated. This strategy of establishing excess synapses *in utero* then systematically removing many of them during postnatal life is thought to allow information from the environment to shape developing circuits. Consistent with this reasoning, while the initial assembly of synapses occurs largely through genetic mechanisms intrinsic to neurons, synaptic refinement is coordinated to a large extent by sensory experience (Hooks and Chen, 2020; Wiesel and Hubel, 1963a, b). Mounting evidence suggests that sensory-dependent (SD) refinement is essential for establishing mature neuronal connectivity, and the importance of this process is further underscored by the association of refinement deficits with neurodevelopmental disorders such as autism and schizophrenia (Feinberg, 1982; LeBlanc and Fagiolini, 2011). At the other end of the lifespan, the aberrant reactivation of refinement mechanisms is thought to exacerbate neurodegenerative conditions associated with synapse loss such as Alzheimer's disease (AD)(Hammond et al., 2019; Hong et al., 2016). However, the cellular and molecular mechanisms underlying the SD refinement of neural circuits remain unclear. In addition to expanding our basic understanding of a critical stage of brain development, defining such mechanisms may lead to the innovation of new therapeutic strategies for correcting circuit wiring deficits underlying neurological disease.

The retinogeniculate circuit of the mouse has emerged as a gold standard for studying the roles of experience in brain development. In this circuit, retinal ganglion cells (RGCs) in the eye relay information about the visual world to downstream structures in the brain by projecting their axons onto excitatory thalamocortical (TC) neurons in the dorsal lateral geniculate nucleus (dLGN) of the thalamus. TC neurons then relay this information to the primary visual cortex for higher order processing (Hong and Chen, 2011). The retinogeniculate circuit has become an important model of neural circuit development because its cellular composition, anatomy, and physiology have been well-characterized, visual experience can be easily controlled, and the system is highly amenable to multiple modes of experimentation. Electrophysiological analyses have shown that retinogeniculate refinement occurs through sensory-independent mechanisms between birth and postnatal day (P)20, but relies upon visual experience

during a critical period that takes place between P20 and P30 (Hooks and Chen, 2006, 2008). During this period, the number of synapses connecting RGCs to TC neurons decreases while the strength of the remaining inputs increases. Although sensory-independent mechanisms of retinogeniculate development that take place prior to P20 have begun to be elucidated, less is known about the mechanisms underlying the critical period of SD refinement in the dLGN.

To shed light on the molecular mechanisms underlying SD refinement, we previously performed a transcriptomic screen for genes that are upregulated in TC neurons in response to visual stimulation (Cheadle et al., 2018). Across the entire transcriptome, this approach identified the gene encoding the cytokine receptor Fibroblast Growth Factor-inducible protein 14 kDa (Fn14, also known as Tnfrsf12a) as the most highly upregulated gene in TC neurons following the acute re-exposure of dark-reared animals to light. Fn14 is a Tumor Necrosis Factor (TNF) Receptor superfamily member that performs a variety of functions outside of the brain, including skeletal muscle remodeling after injury, liver development, inflammation, angiogenesis, and cell migration and motility (Burkly, 2014; Dogra et al., 2007; Jakubowski et al., 2005; Meighan-Mantha et al., 1999; Tran et al., 2006). Fn14 can perform some of these functions in the absence of ligand binding, while other aspects of Fn14 function occur through the extracellular binding of the receptor to its only known ligand, TNF-associated Weak inducer of apoptosis (TWEAK)(Brown et al., 2013; Wiley and Winkles, 2003). In the brain, we have shown TWEAK to be expressed in microglia in response to sensory experience (Cheadle et al., 2020; Kalish et al., 2018). Merging electrophysiological and ultrastructural approaches to assess retinogeniculate refinement in TWEAK and Fn14 knockout (KO) mice, we discovered that TWEAK-Fn14 signaling is dispensable for sensory-independent phases of synaptic refinement prior to P20 but required for SD refinement between P20 and P30. In particular, we found that, at P27, mice lacking either Fn14 or TWEAK maintained an excess of synapses that ultimately failed to strengthen or function properly, reflecting a deficit in synapse elimination in the absence of this pathway (Cheadle et al., 2020; Cheadle et al., 2018). These studies revealed that cytokine signaling between microglia and neurons is critical for SD refinement in the developing brain, and established the TWEAK-Fn14 pathway as an immune signaling mechanism that is repurposed by the brain to sculpt developing circuits in response to experience.

The discovery of the TWEAK-Fn14 pathway as an intercellular signaling axis that is engaged by sensory experience to refine developing circuits presents the opportunity to dissect the downstream mechanisms through which molecular cues from microglia, such as TWEAK, elicit changes in neuronal connections during development. In the periphery, TWEAK and Fn14 coordinate inducible transcriptional programs via the intracellular activation of NfκB and MapK cascades (Brown et al., 2013; Brown et al., 2003; Tran et al., 2006), raising the possibility that microglia-derived TWEAK binds to Fn14 to regulate the expression of genes in TC neurons that are important for synapse elimination. If so, identifying the target genes of TWEAK and Fn14 in TC neurons could reveal a plethora of new mechanisms underlying SD refinement and other aspects of

brain development. Because TWEAK and Fn14 play such a powerful role in circuit development, another question that remains to be addressed is whether this pathway is active selectively in developing visual circuits or instead whether TWEAK and Fn14 represent a more generalizable mechanism governing synaptic connectivity in multiple regions of the developing and mature brain. Finally, whether TWEAK-Fn14 signaling is required for normal brain function and physiology is not yet know. Here, we apply a suite of experimental approaches ranging from single-nucleus RNA-sequencing (snRNAseq) to *in vivo* electroencephalogram (EEG) recordings to further define the mechanisms underlying SD refinement by TWEAK and Fn14, and to elucidate the broader functions of this pathway beyond the dLGN. This work reveals an ability of TWEAK and Fn14 to mediate not only the expression of cytoskeletal synaptic organizers but also of core regulators of the neuronal epigenome, to facilitate memory function, and to protect the brain from seizures and seizure-related mortality. Based upon the increasingly appreciated involvement of pro-inflammatory mechanisms in neurological disease and the likely involvement of Fn14 in AD specifically (Nagy et al., 2021), this work has broad implications for a variety of disorders arising across the lifespan.

Results:

Microglia are required for SD refinement in the dLGN

Work over the past decade has begun to define the many roles of microglia in the healthy brain, from synapse assembly early in circuit construction to synaptic homeostasis and complex behaviors in the adult (Badimon et al., 2020; Miyamoto et al., 2016; Wang et al., 2020). In the dLGN specifically, microglia prune synapses during the first week of life through phagocytic engulfment via localized signaling pathways such as the classical complement cascade (CCC)(Schafer et al., 2012; Stevens et al., 2007). However, microglia engulf synapses to a much lesser extent by the onset of visual experience at eye-opening (P14), leading to the prevailing view that their roles in retinogeniculate refinement are predominantly completed by P20. However, whether microglia are required for SD refinement in the dLGN remains to be tested directly.

To determine whether microglia play a role in SD refinement, we used a pharmacological agent, Plexxikon 5622 (PLX), to deplete microglia from the brain selectively during the critical period of SD refinement in the dLGN (Li et al., 2017). PLX depletes microglia by inhibiting the Colony Stimulating Factor 1 receptor which is necessary for microglial survival. Feeding mice chow formulated with PLX beginning at P18 led to the efficient removal of virtually all microglia from the dLGN by P20 and persisted until the end of the experiment at P27 (Fig. 1A-C). While the drug does not provide a high degree of spatial resolution, with depletion occurring not only in the dLGN but across the entire central nervous system, it has the advantage of tight temporal control, allowing us to restrict microglial depletion to the critical period of SD refinement in the dLGN.

To quantify retinogeniculate synapses in PLX-treated mice versus mice fed with control chow, we performed spine analysis via Golgi staining, a read-out that we previously showed to serve as a structural correlate of functional retinogeniculate synapses (Cheadle et al., 2020). While we did not observe overall differences in the length and width of spines between the two conditions, we found that mice lacking microglia maintained 1.8 times more spines overall than mice with microglia (Fig. 1D,E). Applying our recent definition of the three major spine populations in the dLGN (Cheadle et al., 2020) revealed that microglia-depleted mice maintained 3.2 times more mature, bulbous-shaped spines and 1.7 times more thin-shaped spines but roughly the same number of non-bulbous spines (Figure 1F-H). These data indicate that, consistent with TWEAK-Fn14 signaling from microglia to neurons mediating SD refinement, microglia are required for the elimination of synapses in response to sensory experience.

Whole-transcriptome characterization of Fn14-regulated genes at single-cell resolution

While depletion of microglia using PLX has emerged as a powerful discovery tool for assessing the roles of microglia in the brain, it is a relatively imprecise approach that is prone to initiating compensatory mechanisms, making it difficult to interpret the results of these experiments in the absence of supporting data. To this end, we reasoned that dissecting the downstream mechanisms through which TWEAK-Fn14 signaling disassembles synapses in response to sensory experience may allow for a more precise manipulation of microglial function, providing broad insights into neuro-immune mechanisms of synaptic refinement while also shedding light on the specific mechanisms through which the TWEAK-Fn14 cytokine pathway remodels developing circuits. Given that TWEAK and Fn14 control gene expression in the periphery, we hypothesized that the pathway may also coordinate the induction of transcriptional programs in TC neurons of the dLGN, including genes with as-yet undescribed functions in neural circuit wiring.

Given that Fn14 is the neuronal receptor of the TWEAK-Fn14 pathway, we reasoned that if this pathway regulates neuronal transcription, we would observe robust genetic changes in the TC neurons of mice lacking Fn14. To identify the genes that are regulated by Fn14 in TC neurons in an unbiased manner, we performed single-nucleus RNA-sequencing (snRNAseq) on the dLGNs of Fn14 KO and WT littermates at P27, a time point at which we have shown Fn14 to promote synapse elimination in response to sensory experience (Cheadle et al., 2018). We utilized the inDrops method of high-throughput sequencing to sample the transcriptomes of individual nuclei across two biological replicates of each genotype (Zilionis et al., 2017). After the removal of putative doublets and sequencing read quality control (Fig. S1A-D), we proceeded with downstream analysis of a final dataset of 11,586 nuclei using the R package Seurat v3 (Stuart et al., 2019). Nuclei were assigned to cell types based upon known marker gene expression, with excitatory TC neuron clusters being identified by co-expression of *Slc17a6* (*Vglut2*) and *Prkcd* (Fig. 2A,B and Fig. S2A-G). While the clustering algorithm separated TC neurons into two large and two very small clusters, their separation was based upon relatively subtle transcriptional differences, consistent with prior studies

(Kalish et al., 2018)(https://www.biorxiv.org/content/10.1101/2020.11.05.367482v2). Thus, we focused the bulk of our initial analysis on TC clusters one and two which were sequenced to an average depth of 2985 and 1740 unique molecular identifiers (UMIs) per cell, respectively.

We next utilized the R package Monocle v2 to identify genes that were significantly differentially expressed (differentially expressed genes, DEGs) in WT versus Fn14 KO cells (Qiu et al., 2017). DEG analysis of TC clusters one and two, the larger TC clusters, revealed that gene expression is robustly misregulated in the Fn14 KO mouse. In Fn14 KO cells of TC cluster one, 616 genes were downregulated and 479 genes were upregulated compared to WT at a false discovery rate of less than 5% (FDR < 0.05) and a fold-change threshold of greater than 1.25-fold. In the second TC cluster, 510 genes were downregulated while 237 genes were upregulated in Fn14 KO neurons (Fig. 2C). Since changes in gene expression occurring as an indirect result of circuit immaturity in the Fn14 KO mouse may be expected to exhibit a relatively equal distribution of up- and downregulated genes, the observation that the majority (56% in cluster 1 and 68% in cluster 2) of misregulated genes are downregulated in the KO is consistent with these genes being inducible targets of Fn14-dependent signaling. Another indication that Fn14 actively regulates the expression of these genes is that the vast majority of DEGs in the dataset were observed in TC neurons specifically, which are the sole expressers of Fn14 in the dLGN (Fig. 2C). While we also noted substantial genetic changes in an inhibitory cluster distinguished by high levels of Proenkephalin (*Penk)* expression, fluorescence *in situ* hybridization (FISH) confirmed that these cells predominantly reside in the nearby structures of the ventral LGN and the intergeniculate leaflet which were inadvertently captured in our dLGN microdissection (Fig. S3). Thus, the majority of genetic changes in the dLGNs of Fn14 KO mice involved the downregulation of genes in TC neurons.

We next performed gene ontology analyses to assess the functions of Fn14-regulated genes in an unbiased manner (Mi et al., 2013). We first examined the genes that were significantly downregulated in Fn14 KO mice in both TC clusters one and two, as we reasoned that these genes are most likely to be misregulated as a direct result of Fn14 deletion. Consistent with Fn14 mediating synapse elimination by controlling neuronal transcription, a substantial number of misregulated genes encoded molecules with important functions at synapses. These included genes associated with glutamate receptor signaling (e.g. glutamate receptors *Gria2* and *Grik1*), dendritic spine morphogenesis (e.g. the membrane trafficking protein *Dnm3*), and postsynaptic organization (e.g. cell adhesion molecules *Lrrtm2* and *NrCAM*)(Fig. 2D). Among the molecules encoded by genes in these functional classes, the cytoskeletal regulator Kalirin is a particularly promising candidate effector of SD refinement given its known roles in the activity-dependent plasticity of dendritic spines and the observation that its expression in the developing brain peaks at P28 (Xie et al., 2007). Another gene that stands out as a potential effector of synapse elimination is the cytoskeletal regulator Dock7, mutations in which contribute to epilepsy and deficits in visual function, possibly resulting from an impairment in synapse elimination such as that observed in Fn14 KO mice (Perrault et

al., 2014; Tai et al., 2014). Overall, the genes in these categories represent promising candidate regulators of SD refinement.

While a substantial proportion of Fn14-regulated genes are directly involved in the local remodeling and plasticity of synapses, a separate cohort is specialized to regulate more global aspects of neuronal function. In addition to genes involved in mRNA processing (e.g. the polymerases *Papolg* and *Papola*) and circadian regulation of gene expression (e.g. the polyadenylation factor *Noct*), we found that critical mediators of heterochromatin organization are also significantly downregulated in Fn14 KO mice (Fig. 2D). These include both Hdac1 and -2, enzymes that repress transcriptional activation by removing acetylation marks from histones, and Dnmt3a, a protein that methylates DNA in a postnatal process that establishes stable gene expression as the brain matures (Park and Kim, 2020; Stroud et al., 2017). GO analysis of genes selectively downregulated in Fn14 KO neurons of TC cluster one provided further evidence that intracellular signaling pathways downstream of membrane-bound Fn14 may be master regulators of chromatin organization. Of note, a relatively large number of histone lysine demethylases (KDMs) were found to be downregulated in Fn14 KO neurons, including (KDM)2a, -3a, -4c, -5a, -5b, -5d, -7a, and Jmjd1c (Fig. 2E). Although the expression of these genes is only subtly (but significantly) decreased in the KO mouse, we were able to validate the downregulation of multiple family members (among other genes in the dataset) by qPCR (Fig. 2F). Thus, neuronal KDMs are downregulated when Fn14 expression is eliminated from the brain.

KDM expression in neurons is critical for brain development and function. This specialized class of nuclear enzymes modifies the epigenetic landscape by removing methyl marks from DNA-associated histones, which can either activate or repress transcription depending upon the site of methylation (Hyun et al., 2017). Therefore, increasing KDM expression may be a method whereby Fn14, upon its induction in response to sensory experience, provides feedback to the nucleus to maintain mature synaptic connectivity in the long-term by contributing to the maturation of the epigenetic landscape. Consistent with possible roles for KDMs in SD refinement, members of the Kdm5 and Kdm6 families are required for early neuronal development and Kdm6b, whose expression is induced by neural activity, mediates late stages of synaptic maturation in mice (Hatch et al., 2021; Shen et al., 2014; Wijayatunge et al., 2014; Wijayatunge et al., 2018). Furthermore, *de novo* mutations in *KDM1A*, *KDM6B*, and *KDM5C* have all been linked to neurodevelopmental disorders in humans, consistent with evidence that impairments in SD refinement as well as microglia-neuron signaling contribute to neuropathology (Swahari and West, 2019). In line with Fn14 functioning in part by regulating gene expression in the nuclei of TC neurons through varied mechanisms beyond chromatin remodeling, genes downregulated in cluster one are also enriched for mediators of mRNA splice site selection and RNA export from the nucleus while those in cluster two regulate RNA 3’ end processing and mRNA splicing via the spliceosome (Fig. 2G and H). Thus, Fn14 may regulate the molecular composition of neurons both through the organization of chromatin which may directly shape transcriptional induction, and

through the regulation of RNA production, processing, and export. Altogether, these data reveal an important role for the cytokine receptor Fn14 in positively regulating the expression of genes encoding molecules critical for local changes in synapse number and organization as well as global changes in the epigenetic landscapes of TC neurons in the dLGN. We speculate that the changes in the expression of synapse regulators allow Fn14 to actively eliminate synapses during a critical period of development while the epigenomic changes maintain the established pattern of synaptic connectivity beyond development.

The microglial cytokine TWEAK regulates gene expression in TC neurons of the dLGN

While Fn14 can regulate gene expression in the absence of its ligand TWEAK, TWEAK requires Fn14 to mediate its cellular functions (Brown et al., 2013; Dogra et al., 2007). Therefore, we hypothesized that genetic deletion of TWEAK would also result in the downregulation of genes in TC neurons, some of which may overlap with the genes that are downregulated in TC cells of the Fn14 KO. Given that microglia are the predominant expressers of TWEAK, the genes that are downregulated in TWEAK KO neurons may represent those whose expression is controlled specifically through microglia-neuron signaling. To identify TWEAK-regulated genes, we performed snRNAseq on the dLGNs of TWEAK KO and WT mice across four bioreplicates per genotype using the same approaches as described above. The final dataset included 50,004 nuclei of which we focused the bulk of our analysis on TC neuron cluster two because it exhibited the highest read-depth of TC neuron clusters at 2025.62 UMIs per cell (Fig. 3A,B; Fig. S1E-H; Fig. S2H-O). Identification of DEGs across all cell types using Monocle v2 revealed that, unlike in the Fn14 KO mouse, the changes in gene expression were not primarily observed in TC cells but distributed much more evenly across the diversity of cell types in the dataset (Fig. 3C). Furthermore, whereas deletion of Fn14 predominantly led to decreased gene expression in the Fn14 KO, this was not the case for the TWEAK KO, where the misregulated genes in TC neurons were both up- and downregulated. Consistent with Fn14 mediating synapse elimination both in the presence and absence of TWEAK, the overall numbers of misregulated genes in TC neurons of the TWEAK KO were much lower than in the Fn14 KO, which was particularly striking for the genes that are downregulated in the respective KOs specifically (Fig. 3D). On the other hand, the numbers of genes that were upregulated in Fn14 and TWEAK KO mice were more closely aligned (Fig. 3E).

Thresholding for genes displaying at least a 1.25-fold change in TC neurons of Fn14 or TWEAK KO mice versus WT revealed a low degree of overlap between these gene sets (Fig 3F,G). This result suggests that the bulk of the misregulated genes that we detect in the Fn14 KO neurons may represent those whose expression does not require TWEAK. On the other hand, the genes that are downregulated in TC neurons of the TWEAK KO may represent the gene targets of Fn14 signaling induced specifically by ligand binding. If so, the limited degree of overlap between the gene sets may reflect that TWEAK-dependent aspects of synapse elimination are more nuanced than TWEAK-

independent aspects, consistent with our previous discovery that only a subset of microglia in the dLGN express TWEAK while all TC neurons express Fn14 (Cheadle et al., 2020). Consistent with this possibility, GO analysis revealed that some of the TWEAK-regulated genes encode mediators of the same biological processes as the genes that are regulated by Fn14, while others are predicted to function in distinct but relevant aspects of circuit development. For example, mediators of postsynaptic development and function were not as prevalent among the TWEAK-regulated genes as among Fn14-regulated genes, whereas TWEAK-regulated genes were enriched for putative mediators of presynaptic development such as neuronal process extension and microtubule cytoskeleton organization (e.g. Map1b and several members of the Tubulin family). Additionally, TWEAK-regulated genes were associated with a variety of signaling pathways known to play critical roles in brain development, such as Wnt signaling and the MapK pathway (Fig. 3H). The regulation of MapK signaling is interesting given that this is a pathway through which TWEAK-Fn14 signaling mediates transcription outside of the brain, indicating that TWEAK may serve to provide positive feedback to the pathway in neurons, thereby sustaining transcriptional regulation following TWEAK binding to Fn14.

The most intriguing observation to arise from this analysis was the enrichment of regulators of chromatin assembly and disassembly among TWEAK-regulated genes, indicating that both TWEAK and Fn14 couple SD refinement to long-term changes in the epigenomic landscape (Fig. 3H). While the chromatin modifiers that are misregulated in TWEAK KO neurons are distinct from those that are misregulated in the absence of Fn14, several important functional parallels emerge. For example, whereas Fn14 regulates the expression of Hdacs which remove acetylation marks from histones thereby repressing transcription, TWEAK regulates the expression of Set, which can inhibit the acetylation of histones before it occurs (Bannister and Kouzarides, 2011; Bryk et al., 2002; Kim et al., 2013). TWEAK also regulates the expression of two members of the SWI/SNF nuclear complex of chromatin remodelers, *Smarcc2* and *Arid1a*, which regulate the function of enhancers through various mechanisms (Alver et al., 2017). Mutations in members of the SWI/SNF family, which interact with the activity-dependent AP-1 factor Fos, are strongly associated with neurodevelopmental disorders such as autism which are also associated with both SD refinement and microglial dysfunction (Bogershausen and Wollnik, 2018; Sokpor et al., 2017; Vierbuchen et al., 2017). Overall, these data suggest that the TWEAK-Fn14 pathway mediates SD refinement not only by coordinating the expression of direct regulators of synapse and neuronal development as expected, but also by inducing histone modifications and chromatin remodeling to shape the epigenomic and transcriptomic landscape of dLGN TC neurons in the long-term.

Given that TWEAK-Fn14 signaling occurs at the cell membrane and induces genetic changes via the activation of intracellular pathways rather than through direct binding to DNA, we next sought to harness our transcriptomic data to garner insights into the specific transcription factors (TFs) that may coordinate the genetic changes observed in TWEAK and Fn14 KO mice. To this end, we performed an unbiased motif enrichment

368 analysis to identify DNA sequences that were enriched in regions within 200 kb upstream
369 and downstream centered on the transcriptional start sites of the genes that were
370 downregulated in TC neurons of either KO mouse line. In all cases, motifs predicted to
371 bind several TFs were identified, with Irf3, Ets2, and Sp4 being particularly highly
372 represented in the data (Fig. S4). The same TFs were implicated in both TWEAK- and
373 Fn14- KO datasets, suggesting that, although Fn14 KO and TWEAK KO mice displayed
374 largely distinct sets of misregulated genes, the transcriptional regulators expected to
375 govern over these distinct gene programs were largely the same. This result is consistent
376 with TWEAK mediating gene expression solely through binding to Fn14. Altogether, these
377 snRNAseq data, described in Supplemental tables 1 – 4 with unprocessed read files
378 uploaded to GEO (submission pending), suggest that TWEAK-Fn14 signaling regulates
379 SD refinement at least in part by controlling the molecular composition of developing TC
380 neurons.

381 *Fn14 expression extends to glutamatergic neurons throughout the developing and mature*
382 *brain*

383 TWEAK and Fn14 play a powerful role in SD refinement in the developing dLGN,
384 and the data described above indicate that one mechanism of action is through
385 transcriptional regulation of genes with critical roles in neurons. Our observations in the
386 dLGN coupled with a recent study describing a role for TWEAK in dampening long-term
387 potentiation in the mature hippocampus (Nagy et al., 2021) led us to explore whether
388 TWEAK-Fn14 signaling may be important for non-visual aspects of brain connectivity and
389 function. To assess this possibility, we first visualized Fn14 expression across the entire
390 mouse brain using multiplexed FISH (RNAscope) of sagittal sections from mice during
391 peak SD refinement at P28, as well as at P90 after the brain has fully matured.

392 At both P28 and P90, Fn14 expression was restricted to precise neuronal
393 populations across a variety of brain structures, with expression generally increasing
394 along an anterior-to-posterior axis (Fig. 4A,B). Fn14 expression was particularly high in
395 the cerebellum where it was largely restricted to the granule cell layer, the brain stem, the
396 thalamus, and within select cells in the hippocampus and cortex. In the dLGN, we
397 observed *Fn14* expression predominantly within *Vglut1*+ TC neurons (89.4% of *Fn14*+
398 cells were *Vglut1*+)(Fig. 4C,D), as previously described and consistent with the
399 misregulation of gene expression in this cell type upon deletion of *Fn14* (Cheadle et al.,
400 2018). The hippocampus exhibited similar co-expression of *Vglut1* and *Fn14* such that
401 ~80% of *Fn14*+ cells in CA1, CA3, and the dentate gyrus also expressed *Vglut1*.
402 Furthermore, analysis of *Fn14* mRNA at P90 revealed that *Fn14* expression is retained
403 in glutamatergic neurons across all regions analyzed as the brain matures (Fig. 4D). We
404 also observed a small subset of *Gad1*+ inhibitory neurons that expressed Fn14 (6.19%)
405 predominantly within the hippocampus at both ages (Fig. S5). Inhibitory neurons in the
406 hippocampus represent only 10-15% of the neural population yet exert large-scale control
407 over hippocampal synchrony, function, and circuit development (Pelkey et al., 2017). We
408 found that these rare *Fn14*+ inhibitory neurons expressed equal amounts of *Fn14* as the

Fn14+ glutamatergic neurons, indicating that Fn14 is not limited to excitatory populations in the hippocampus as it is in the dLGN (Fig. 4E). Nevertheless, there is a significantly stronger relationship between *Fn14* and *Vglut1* than between *Fn14* and *Gad1*, suggesting that Fn14 functions predominantly in glutamatergic neurons (Fig. 4F). Altogether, these results suggest that the functions of TWEAK-Fn14 signaling extend beyond the developing visual system and may be relevant to mature brain function as well.

Fn14 is dispensable for learning but required for memory task proficiency

While the roles of microglial cytokine signaling in the healthy brain have been most extensively studied in the context of synapse elimination during development, several recent studies have suggested that these pathways also play a role in maintaining circuit homeostasis, excitatory/inhibitory balance, and even complex behaviors in the adult (Badimon et al., 2020; Nguyen et al., 2020; Wang et al., 2020). We speculate that some of the mechanisms underlying synapse refinement during development may also underlie synaptic plasticity in the mature brain. Given the expression of Fn14 in excitatory neurons of the hippocampus, a brain region that is critical for both learning and memory and the function of which can be assayed robustly using well-defined behavioral tests, we next sought to determine whether Fn14 facilitates hippocampal function in adult mice.

We tested the roles of Fn14 in learning and memory using two well-established tasks: cued fear conditioning (CFC) and Morris water maze (MWM). In the CFC task, we examined the abilities of Fn14 KO and WT littermates to associate both an auditory cue and a spatial context with a paired aversive foot shock (Fig. 5A). During the initial conditioning phase, when the foot shock was accompanied by a tone (75 dB; 2000 Hz) and a novel arena (striped walls and floor grating), both Fn14 KO and WT mice exhibited a stereotyped freezing response reflecting fear of the shock (Fig. 5B). Similarly, when mice of both genotypes were placed into a novel context (a round arena with polka dotted walls) without a tone, they exhibited low levels of freezing. However, loss of Fn14 resulted in a trending decrease in freezing when re-exposed to the paired context but not the tone (context (-) tone condition), and a significant decrease in freezing when the novel context was paired with the associated tone (novel context +tone)(Fig. 5B). These results suggest that Fn14 KO mice did not sufficiently retain the memory that the tone was paired with a foot shock. While this deficit was observed both for the spatial context and the auditory tone, it was particularly robust when only the tone was displayed.

Because impairments in the CFC task could reflect functional changes in the amygdala or the frontal cortex in addition to the hippocampus, we next assessed the effect of loss of Fn14 on a more purely hippocampal-dependent spatial learning task, the MWM (Fig. 5C). In this task, the mice were placed in a round pool with each cardinal direction being marked by a distinctive shape to allow for spatial mapping of the arena. During the initial visible training stage, WT and Fn14 KO mice were both able to effectively locate a visible goal platform. After mice were trained to perform the task, the water in the pool was made opaque, and the goal platform submerged, forcing mice to orient themselves using the spatial cues to locate the goal platform rather than the platform itself. On all trials in which the platform was hidden, WT and Fn14 KO mice learned to find the platform equally well as revealed by their similar latencies to reach the platform

452 and the lengths of the paths that they took to reach it (Fig. 5D; Fig. S6). Thus, as also
453 demonstrated by the results of the CFC task, loss of Fn14 does not have a strong
454 observable effect on learning.

455 To specifically assess memory function, we next tested whether, after a period of
456 24 hours, the mice remembered the location of the hidden platform. When the platform
457 was removed from the pool in probe trials, WT mice swam a significantly greater distance
458 in the quadrant where the platform was previously hidden than Fn14 KO mice, suggesting
459 that WT mice were able to remember the spatial location of the platform while mice lacking
460 Fn14 were unable to remember the goal location (Fig. 5E). This deficit was not caused
461 by a motor impairment, as WT and Fn14 KO mice swam an equal distance overall during
462 the probe trial (Fig. 5F). Following the probe trials, the goal platform was reintroduced into
463 the pool, but now in the opposite quadrant of the arena. Just as in the hidden trials, both
464 WT and Fn14 KO mice were able to locate and learn the new reversed goal zone equally
465 well, again suggesting that Fn14 does not affect learning. Rather, the specific deficits
466 observed in the probe trials suggest that loss of Fn14 impairs long-term memory in this
467 hippocampal-dependent task.

468 In order to determine the microglial contribution to the memory deficits caused by
469 loss of Fn14 signaling, we next tested PLX-administered, microglia-depleted mice in both
470 CFC and MWM. As with Fn14 KO mice, PLX mice froze to the same extent as control
471 mice during initial conditioning to the averse stimulus as well as when placed in the novel
472 context (Fig. S7A). PLX-administered mice also froze to an equal extent as control mice
473 when the mice were re-exposed to the conditioned context but not the tone. Interestingly,
474 there was a trending decrease in freezing in PLX mice when they were re-exposed to the
475 conditioned tone in a novel context ($p = 0.0989$), which was the condition with the greatest
476 effect size in Fn14 KO mice (Fig. S7A). This result suggests that this aspect of the
477 memory deficit in mice lacking Fn14 may be related to aberrant TWEAK signaling from
478 microglia. Nevertheless, microglial depletion did not significantly affect performance in the
479 MWM task, confirming that some aspects of Fn14 function do not require TWEAK (Fig.
480 S7B-H). Overall, these data suggest a critical role for Fn14 in memory but not learning,
481 consistent with our previous findings that synapses in the Fn14 KO mouse fail to properly
482 strengthen (Cheadle et al., 2018).

483 *Loss of Fn14 exacerbates PTZ-induced seizures*

484 In combination with recent studies demonstrating a requirement of TWEAK and
485 Fn14 for visual circuit development and hippocampal plasticity, our findings that Fn14
486 mediates the expression of neuronal transcription and is required for memory suggest
487 that this pathway is critical for mature brain function. Thus, we next sought to determine
488 whether Fn14 regulates overall (i.e. gross) neural activity in adult mice *in vivo*. Using
489 electroencephalogram (EEG) probes implanted into the dorsal skull, we quantified the
490 effect of loss of Fn14 on brain activity over a 48-hour period (Fig. 6A). To ensure the mice
491 had similar baseline physiology, the animals' overall locomotor activity and body
492 temperature were monitored. Fn14 KO and WT mice exhibited equal body temperature

493 and activity levels over the recording session (Fig. S8), similarly to what we observed in
494 the MWM task (Fig. S6). Correspondingly, we found that there was no difference in
495 average EEG spectral power between Fn14 KO and WT mice in delta (1-4 Hz), theta (4-
496 8 Hz), alpha (8-12 Hz), beta (12-30 Hz), low gamma (30-60 Hz) and high gamma (60-90
497 Hz) frequency bands (Fig. 6B). Therefore, as implicated by the normal performance of
498 mice lacking Fn14 in the learning phases of both the CFC and the MWM, loss of Fn14
499 does not affect baseline neural activity on a gross level.

500 Consistent with Fn14 functioning at least in part downstream of microglial
501 cytokines, studies using PLX to deplete microglia also found that PLX-treated mice did
502 not exhibit baseline changes in EEG spectral power across the range of relevant bands
503 overall. Rather, microglial depletion resulted in increased seizure risk when mice were
504 challenged with a neural stimulant (Badimon et al., 2020). Given that mice without
505 microglia maintain an excess of synapses due to deficits in synapse elimination which are
506 also observed in Fn14 KO mice (Fig. 1)(Cheadle et al., 2020), we wondered whether loss
507 of Fn14 would lead to a similar susceptibility to seizures. To determine whether loss of
508 Fn14 confers seizure risk, we analyzed the responses of Fn14 KO mice to the $GABA_a$
509 antagonist pentylenetetrazole (PTZ), a convulsant agent used to elicit seizures (Van Erum
510 et al., 2019). Intraperitoneal injection of PTZ (60 mg/kg) into Fn14 KO and WT mice time-
511 locked with EEG recordings demonstrated profound differences in the responses of mice
512 of each genotype to PTZ (Fig. 6C). Upon PTZ injection, Fn14 KO mice were more likely
513 than WT littermates to develop general tonic clonic (GTC) seizures, and KO mice
514 developed GTCs at a shorter latency than WT mice (Fig. 6D-E). Furthermore, GTC
515 seizures had a longer duration in Fn14 KO mice (Fig. 6C,F) when compared to GTCs in
516 WT mice. Concurrently with the increase in GTC severity, Fn14 KO mice had a
517 significantly higher mortality rate after PTZ challenge than WT mice (Fig. 6H).
518 Interestingly, Fn14 KO mice experienced significantly fewer myoclonic seizures than WT
519 mice (Fig. 6G), potentially due to the higher mortality of Fn14 KO mice. Lastly, loss of
520 Fn14 led to a worse overall seizure phenotype as scored by a combination of their
521 recorded behavior, EEG activity, and mortality, suggesting that loss of Fn14 confers an
522 increased susceptibility to acutely induced seizures (Fig. 6I). Altogether, these functional
523 data reveal that, although Fn14 KO mice do not exhibit overt deficits in their brain activity
524 at baseline, upon increasing excitatory tone through PTZ-mediated disinhibition, loss of
525 Fn14 greatly exacerbates seizure severity and worsens seizure outcomes. Thus, Fn14 is
526 not only necessary for neural circuit development, it is a core regulator of neural activity
527 and function in the mature brain.

528 **Discussion**:

529 Over the past several years, it has become increasingly evident that cytokine
530 signaling pathways play essential roles in the organization of neural circuits in the
531 developing and mature brain (Ferro et al., 2021). However, we are still in the early stages
532 of defining the downstream mechanisms through which these pathways shape neuronal
533 connectivity in the long-term. Here, we derive significant insights into how a TNF-family

534 cytokine signaling axis that mediates inflammation outside of the brain, the TWEAK-Fn14
535 pathway, also controls a postnatal stage of circuit refinement through the coordination of
536 gene expression in excitatory TC neurons of the dLGN. We further show that expression
537 of Fn14 extends to excitatory neurons across a diversity of non-visual structures in the
538 developing and mature brain, suggesting that Fn14 and its ligand TWEAK coordinate
539 multiple aspects of brain function, many of which likely remain to be identified. Supporting
540 this possibility, behavioral analysis revealed that Fn14 is dispensable for learning but that
541 loss of Fn14 impairs memory. This observation is consistent with previous reports that
542 synapses do not strengthen properly in the absence of Fn14 (Cheadle et al., 2018), and
543 that synaptic plasticity in the hippocampus is impaired when TWEAK-Fn14 signaling is
544 manipulated (Nagy et al., 2021). Finally, we demonstrate that, while mostly normal at
545 baseline, seizure activity in mice lacking Fn14 is excessively heightened upon exposure
546 to a convulsant, leading to a strikingly high mortality rate in mice lacking Fn14. Overall,
547 this multi-disciplinary study elucidates the roles of TWEAK-Fn14 signaling in the brain
548 from the regulation of genes encoding effectors of synaptic and epigenomic remodeling
549 during development to brain-wide activity and cognitive function in the adult.

550 While classically associated with the brain's response to injury and inflammation,
551 work over the past 10 years has begun to define key roles for microglia—and the cytokine
552 signaling pathways that they engage—in the healthy brain (Paolicelli et al., 2011). For
553 example, in the retinogeniculate system, microglia coordinate an early phase of synaptic
554 pruning that occurs during the first week of life (well before the onset of sensory
555 experience at eye-opening) and involves the phagocytic engulfment of synapses through
556 local microglia-neuron interactions mediated by the classical complement cascade
557 (CCC)(Schafer et al., 2012; Stevens et al., 2007). The engagement of immune signaling
558 pathways—such as the CCC, chemokines, Interleukins, and C1q-like proteins—that
559 function locally at contact points between microglia and synapses has since emerged as
560 a major theme in microglial regulation of brain wiring (Gunner et al., 2019; Kakegawa et
561 al., 2015; Paolicelli and Gross, 2011; Vainchtein et al., 2018). TWEAK-Fn14 signaling is
562 unique among these pathways in that TWEAK and Fn14 coordinate a late phase of
563 retinogeniculate refinement that takes place after eye-opening and is driven by sensory
564 experience, a process that we show here to require microglia (Fig. 1)(Cheadle et al., 2020;
565 Cheadle et al., 2018). While TWEAK and Fn14 represent the first cytokine signaling
566 mechanism shown to underlie SD refinement in the retinogeniculate circuit, work in other
567 systems corroborates that microglia and immune signaling pathways can function in an
568 experience-dependent manner. For example, microglia employ fractalkine signaling to
569 prune thalamic inputs to somatosensory barrel cortex in response to whisker lesioning
570 (Gunner et al., 2019), and microglia engulf extracellular matrix components to facilitate
571 synaptic plasticity in the hippocampus via environmentally induced IL-33 signaling
572 (Nguyen et al., 2020). Here, we expand upon data that demonstrates roles for cytokine
573 signaling in SD features of brain development and plasticity in the visual system by
574 defining the downstream mechanisms of cytokine action.

575 The complex architecture of the brain is likely to be constructed through a multitude
576 of signaling mechanisms beyond the pathways that have been the focus of neuroscience
577 research for many decades (e.g. Ephrin/Eph and Semaphorin/Plexin signaling). As
578 discussed above, the diverse array of cytokine signaling molecules that coordinate innate
579 immune responses in the periphery are promising candidates to regulate aspects of
580 neural circuit wiring. Brain-specific roles for TWEAK and Fn14 in particular highlight
581 intriguing functional parallels between the immune system and the nervous system,
582 exemplifying how both of these systems being specialized to respond to changes in the
583 external environment (i.e. viral/bacterial infections or sensory stimulation, respectively).
584 Notably, roles for Fn14 and TWEAK in the brain to some extent mimic their roles in the
585 process of non-neural tissue remodeling following injury. Two key features of Fn14
586 function are conserved across these different biological contexts: (1) expression of Fn14
587 is low in normal tissue but dramatically increased by injury or pathology in the periphery
588 (or neuronal activity in the brain), and (2) TWEAK released from innate immune cells in
589 the local environment, i.e. macrophages or microglia, binds Fn14 upon its upregulation to
590 drive tissue or circuit remodeling in the long-term. These aspects of TWEAK-Fn14
591 function begin to explain how the pathway can be neuroprotective when expressed at low
592 levels in the resting brain but inflammatory and damaging when chronically upregulated
593 by injury or neurodegenerative disease (Nagy et al., 2021). Our finding that TWEAK and
594 Fn14 promote circuit development at least in part through transcriptional regulation
595 represents another parallel between the roles for TWEAK and Fn14 in peripheral
596 immunity and neurological function. Broadly, our work suggests that, as neuroscientists
597 continue to identify cytokine signaling pathways that have important functions in the brain,
598 elucidating how these pathways organize brain connectivity could likely be accelerated
599 by considering how they function in the context of innate immunity.

600 Consistent with cytokine function extending beyond local signaling mechanisms,
601 the work presented here demonstrates that TWEAK and Fn14 can elicit global changes
602 in the transcriptomic landscapes of neurons to wire circuits in the long-term. While our
603 finding that TWEAK-Fn14 signaling mediates the expression of active effectors of
604 synapse remodeling is consistent with the known functions of this pathway in SD
605 refinement, we were surprised to find that TWEAK and Fn14 also control the expression
606 of a large number of chromatin regulators in the neuronal nucleus. We speculate that the
607 regulation of genes encoding synaptic cytoskeletal regulators like Kalirin and Dock7 may
608 facilitate the active sculpting of circuits during the critical period of refinement, while the
609 regulation of heterochromatin organizers such as KDMs and Hdacs serves to shape the
610 epigenomic landscape more globally, possibly to initiate gene programs and then solidify
611 TWEAK- and/or Fn14-dependent changes in circuit connectivity and gene expression
612 such that they persist into maturity. Consistent with this idea, the critical period of SD
613 refinement in the visual system corresponds with a developmental process of epigenetic
614 maturation that involves permanent changes to the neuronal epigenome, impairments in
615 which can lead to neurodevelopmental disorders such as intellectual disability and autism
616 (Kalish et al., 2018; Stroud et al., 2017; Stroud et al., 2020). Our work provides the first
617 evidence that neuro-immune signaling interactions, i.e. TWEAK-Fn14 signaling, are

engaged by sensory experience to regulate the establishment of the mature neuronal epigenome. In the future, genomic studies in mice conditionally lacking TWEAK and Fn14 from microglia and excitatory neurons, respectively, will be applied to more directly determine whether the transcriptional regulation of heterochromatin organizers by this pathway leads to changes in histone modification and chromatin organization within neurons during development and in the adult. More extensive analyses of the large-scale transcriptomic datasets that we have produced here (Supplemental Tables 1-4, GEO submission pending) may also shed light on this gap in knowledge. Finally, given that the genes that are misregulated in the TWEAK and Fn14 KO mouse lines are largely distinct, it will be important to disentangle which of the genetic mechanisms we have identified rely upon signaling from microglia to neurons and which may be neuron-intrinsic.

Compared to the roles of microglia and cytokines in brain development, less is known about the ongoing functions of cytokines in the mature brain. This is a critical gap in knowledge to address given that neuroinflammation is associated with a broad range of neurological disorders emerging after development, such as multiple sclerosis, stroke, and neurodegeneration. In addition to a possible role for TWEAK and Fn14 in neurodevelopmental disorders, data also suggest that TWEAK-Fn14 signaling may be particularly relevant in the context of Alzheimer's disease (AD), which is thought to be exacerbated by the aberrant re-activation of refinement mechanisms in the mature brain (Hammond et al., 2019; Hong et al., 2016). Fn14 expression is heightened in brain tissue from individuals with AD, and a recent study showed that inhibiting TWEAK-Fn14 signaling using a TWEAK-blocking antibody rescues synaptic plasticity deficits in a well-established mouse model of AD (Nagy et al., 2021). Our data support a potential role for heightened TWEAK-Fn14 signaling in disorders of cognition and memory, including AD, by demonstrating that Fn14 is expressed in the hippocampi of adult mice, and that loss of Fn14 results in impaired memory in multiple hippocampal-dependent tasks. Based upon these data, we speculate that TWEAK-Fn14 signaling may be a druggable therapeutic target for treating neurological disorders across the lifespan including AD. In future studies, we will explore the ability of small molecule inhibitors of TWEAK-Fn14 signaling to ameliorate neuropathology in mouse models of neurological disorders with the ultimate goal of targeting this pathway as a new therapeutic strategy for treating brain disease.

Acknowledgements:

We acknowledge Drs. Linda C. Burkly (Biogen), Sameer Dhamne (Boston Children's Hospital), Jessica Tollkuhn (Cold Spring Harbor Laboratory), Timothy Cherry (Seattle Children's Hospital), Jacqueline Barker (Drexel University), Elizabeth Pollina (Harvard Medical School), Marija Cvetanovic (University of Minnesota) and Cody Walters (Nature Communications) for thoughtful discussions and feedback on the study. Work in this study was aided by the Single-Cell core facility at Harvard Medical School and the Behavior and Physiology core at Boston Children's Hospital.

Funding:

This work was supported by a R00 MH120051-4 (NIMH), a McKnight Scholar Award, a Rita Allen Scholar Award, and a Klingenstein-Simons Fellowship in Neuroscience (to L.C.).

Author Contributions:

L.C. conceptualized the study. L.C., A.F., U.V., and Y.S.S.A. performed experiments. L.C. analyzed snRNAseq and spine data. A.F. analyzed FISH, behavioral, and EEG data. U.V. analyzed qPCR and immunostaining under the guidance of A.F. Y.S.S.A. performed motif enrichment analyses, tissue processing, and mouse line maintenance. L.C. and A.F. wrote the manuscript with input from U.V. and Y.S.S.A.

Conflicts of Interest:

The authors report no conflicts of interest.

STAR Methods:

Animal models

All experiments were performed in compliance with protocols approved by the Institutional Animal Care and Use Committee (IACUC) at Harvard Medical School and Cold Spring Harbor Laboratory. The following mouse lines were used in the study: C57Bl/6J (the Jackson Laboratory, JAX:000664); B6.Tnfrsf12a$^{tm1(KO)Biogen}$ (Fn14 KO)(Jakubowski et al., 2005); and B6.Tnfsf12$^{tm1(KO)Biogen}$ (TWEAK KO)(Dohi et al., 2009). TWEAK and Fn14 KO mice were generously provided by Dr. Linda Burkly at Biogen (Cambridge, MA) and are subject to a Material Transfer Agreement with Cold Spring Harbor Laboratory. Analyses were performed on equal numbers of male and female mice at postnatal days (P)27 or P90. No sex differences were observed in the study.

Sensory deprivation and stimulation paradigm

In most cases, mice were housed according to a standard 12-hour light/dark cycle at all times. For the late-dark-rearing (LDR) paradigm, C57Bl/6J pups were bred in-house or obtained from The Jackson Laboratory and housed with moms under standard light/dark conditions until P20, at which time they were weaned and moved into the dark, light-proof chamber of a ventilated cabinet. At P27, some of the mice were moved into a separate, well-lit compartment of the cabinet for re-exposure to light for eight hours. Conversely, dark-reared, unstimulated control animals were euthanized by isoflurane and the brains removed in the dark by an investigator using night-vision goggles. Fresh brain tissue was processed for Golgi staining as described below.

Plexxikon 5622 Administration

Chow formulated to contain 1200 mg/kg free base Plexxikon 5622 (PLX; Chemgood, Inc.) was fed to mice between P18 and P27. Control mice were fed chow containing the same ingredients and produced in parallel with PLX-formulated chow, but not containing

697 PLX. All chow was produced and irradiated by Research Diets, Inc. and stored at 4°C.
698 PLX treatment did not cause observable changes in animal health or behavior. As per
699 our standard protocol, mice were fed on the chow *ad libitum* and the investigator
700 provided all husbandry for the mice during treatment.

701 ***Golgi Staining***
702
703 Golgi staining was performed with the FD Rapid GolgiStain kit (FC Neurotechnologies,
704 Inc) according to the manufacturer's protocol. Following sample processing, dendritic
705 segments were traced in x, y, and z planes using a Zeiss Axioskop microscope (63X
706 objective) and Neurolucida (Microbrightfield Bioscience). Spines were categorized
707 based upon parameters determined in a previous study (Cheadle et al., 2020). Example
708 images of spines were obtained on an Olympus BX63 fluorescence microscope with a
709 100X objective.

710 ***Immunofluorescence***
711
712 To validate microglial depletion, PLX-fed and control mice were perfused with ice cold
713 PBS (Gibco) and 4% for paraformaldehyde (PFA), then the whole brains were
714 harvested and post-fixed for 12 hours. After fixation, tissue was incubated in 15% and
715 then 30% sucrose solution before being embedded in OCT (-80°C). Embedded tissue
716 was sectioned coronally at 25 µm thickness onto Superfrost Plus slides using a Leica
717 CM3050 S cryostat. Sections were then washed in PBS and blocked in blocking
718 solution (PBS adjusted to 5% normal goat serum [NGS] and 0.3% Triton X-100 [TX-
719 100]) for 1 hour at room temperature before being incubated in primary antibody
720 solution containing Rabbit-anti-Iba1 (Wako 019-19741, [1:1500]) diluted in PBS with 5%
721 NGS and 0.1% TX100 (probing solution). Sections were incubated in primary antibody
722 overnight at 4°C. The next day, sections were washed 3 times for 10 minutes per wash
723 in PBS before incubation in secondary antibody Alexafluor 488 goat anti-rabbit (Abcam
724 150077; [1:500]) diluted in probing solution for 2 hours at room temperature. Sections
725 were then washed in PBS, covered with DAPI fluoromount-G (SouthernBiotech), and
726 cover-slipped.
727
728 Confocal images (20X) were acquired using a LSM 710 Zeiss microscope and the
729 number of microglia/dLGN was quantified using ImageJ. A total of 3 mice per condition
730 and a minimum of two images per mouse were analyzed. In some cases, we increased
731 the contrast across and subtracted the background across an entire image to clarify the
732 features of interest that are presented in the figures. Other than contrast enhancement
733 applied across the entire image, no other manipulations to images were made.
734

735 ***Single-nucleus RNA-sequencing***
736
737 *Tissue preparation, nuclear capture, and next-generation sequencing*:
738
739 Fn14 KO and WT littermate mice and TWEAK KO and WT littermate mice at P27 were
740 euthanized and their brains harvested in ice cold PBS (Gibco). Coronal sections of 300

741 µm were made on a VT1000S vibratome (Leica) in ice cold PBS and the dLGNs were
742 micro-dissected using a Nikon SMZ10A brightfield dissection microscope. Dorsal-LGN
743 tissue from three mice per condition per replicate was pooled and homogenized in HB
744 buffer containing .25 M sucrose and (in mM): 25 KCl, 5 $MgCl_2$, 20 Tricine-KOH, pH 7.8.
745 and 2.5% Igepal-630 (Sigma). HB was adjusted to contain 1 mM DTT, .15 mM
746 spermine, and .5 mM spermidine along with phosphatase and protease inhibitors
747 (Roche). All steps were performed on ice. Following homogenization, the homogenate
748 was layered atop a 30%-40% iodixanol gradient and centrifuged in an SW-41 swing
749 bucket rotor (Beckman) at 10,000*g* for 18 minutes. Small volumes of Bovine Serum
750 Albumin (BSA; Sigma) and RNAsin (Promega) were included in HB and iodixanol
751 solutions. Nuclei were recovered from the 30%-40% iodixanol interface and individual
752 nuclei were captured within microfluidic droplets alongside barcoded hydrogels via the
753 inDrops approach (Zilionis et al., 2017). After cell encapsulation, primers were released
754 by UV exposure. Libraries of 2500 – 3000 nuclei were generated for each sample (one
755 library per bioreplicate for two bioreplicates total of the Fn14 WT/KO line (four libraries
756 total) and two libraries per bioreplicate for four bioreplicates of the TWEAK WT/KO line
757 (16 libraries total)). Indexed libraries for each mouse line were independently pooled
758 and sequenced twice on a Next-Seq 500 (Illumina) with sequencing parameters set at
759 Read 1, 54 cycles; Read 2, 21 cycles; Index 1, 8 cycles; Index 2, 8 cycles.
760
761 *Data processing and analysis*:
762
763 Reads were mapped against a custom transcriptome built from Ensemble GRCm38
764 genome and GRCm38.84 annotation using Bowtie 1.1.1, after filtering the annotation gtf
765 file (gencode.v17.annotation.gtf filtered for feature_type = “gene”, gene_type =
766 “protein_coding” and gene_status = “KNOWN”). Read quality control and mapping were
767 performed. Sequence reads were linked to individual captured molecules by unique
768 molecular identifiers (UMIs). Default parameters were used unless stated explicitly.
769 These steps were previously described (Cheadle et al., 2018; Macosko et al., 2015).
770
771 *Quality control, cell clustering, and differential gene expression analysis*:
772
773 All Fn14 KO/WT nuclei were combined into a single dataset and the same was done for
774 TWEAK KO/WT nuclei, because these experiments were performed separately. The
775 Fn14 and TWEAK datasets were analyzed in parallel using the same approach. First,
776 the R package DoubletFinder (https://github.com/chris-mcginnis-
777 ucsf/DoubletFinder)(McGinnis et al., 2019) was applied to each sample separately to
778 predict and remove potential doublets from the dataset. This step is crucial for ensuring
779 that none of the nuclei in the final dataset actually represent two nuclei encapsulated
780 within the same droplet, which could skew both the analysis and the interpretation of
781 results. This step removed roughly 6% of the nuclei from the dataset. Next, Seurat
782 version 3 was used to further filter out nuclei that may represent surviving doublets or
783 that may be dead or dying cells by removing all nuclei from the dataset that did not
784 contain between 250 and 3,000 UMIs and also removing cells containing greater than
785 5% mitochondrial read counts (Stuart et al., 2019). In Seurat v3, the data were log
786 normalized and scaled to 10,000 transcripts per cell, and variable genes were identified

using default parameters. We limited the analysis to the top 30 principal components (PCs). Clustering resolution was set between 0.5 and 1.0. Clusters containing fewer than 100 cells were removed from the dataset, as were clusters expressing more than one known marker gene. Known marker genes were used to assign clusters to cell types as follows: excitatory thalamocortical neurons, *Slc17a6* and *Prkcd*; all inhibitory neurons, *Gad2*; dLGN-surrounding inhibitory neurons, *Penk*; dLGN-resident inhibitory neurons, *Chrnb3*; oligodendrocytes, *Olig1*; oligodendrocyte precursor cells, *Pdgfra*; astrocytes, *Aqp4* and *Aldoc*; microglia, *P2ry12*; endothelial cells, *Cldn5*; and pericytes, *Vtn*. Excitatory relay neurons, the primary focus of the study, represented ~51% of 11,586 total nuclei in the Fn14 WT/KO dataset and 47% of 50,004 nuclei in the TWEAK WT/KO dataset.

To identify genes that were differentially expressed between KO and WT conditions within a given cell class, we used Monocle 2 (https://github.com/cole-trapnell-lab/monocle2-rge-paper), an R package specialized for quantitative analysis of single-cell data (Qiu et al., 2017). Genes whose differential gene expression false discovery rate (FDR) was less than 0.05 (FDR < 0.05) were considered statistically significant. General descriptions of differentially expressed genes are also based upon a fold-change cutoff of 1.25-fold.

Gene ontology (GO) analyses were performed based upon PANTHER term enrichment on genes that were significantly downregulated in TWEAK or Fn14 KO nuclei with FDR < 0.05 regardless of absolute fold change (Mi et al., 2013). Transcription factor motif enrichment was performed using AME-MEME on the same genes used in GO analysis. Sequences that were input into the MEME-AIM (https://meme-suite.org/; McLeay et al., 2010) represented 400 bp sequences centered on the transcriptional start site of a given differentially expressed gene. Shuffled sequences served as background controls.

RNA isolation and qPCR

Fn14 KO and WT littermate mice and TWEAK KO and WT littermate mice at P27 were euthanized and their brains were bisected and flash frozen using liquid nitrogen in 1 mL of Trizol (Ambion) and kept at -80°C until processing. Tissue was then homogenized using a motorized tissue homogenizer (Fisher Scientific) in a clean, RNAase-free environment. Once homogenized, 200 µL of chloroform was added to each sample and, after thorough mixing, samples were centrifuged at 21,000x*g* for 15 minutes for phase separation. The colorless phase was then collected and combined with equal volumes 70% ethanol and used as input in the RNeasy Micro kit (Qiagen), where we followed the manufacturer's instructions. RNA concentration was then determined using a nanodrop (ND 1000; NanoDrop Technologies inc), and once RNA samples were diluted to equal concentrations, samples were converted into cDNA using SuperScript™ III First-Strand Synthesis System (Thermo Fisher) following the manufacturer's instructions. Specific genes were then amplified (forward and reverse primers can be found in supplemental table 5) and detected using Power Up Sybr Green (Thermo Fisher) in a Quant Studio 3 Real-Time PCR system (Thermo Fisher). Crossing threshold (Ct) values were calculated using the QuantStudio program and relative expression, $2^{-\Delta\Delta Ct}$, was calculated using *GAPDH* as a reference control.

832 ***Single-molecule fluorescence in situ hybridization (FISH)***

833 WT C57Bl/6J mice at either P28 or P90 were euthanized and brain tissue was
834 immediately harvested and frozen at -80°C in OCT (Tissue-Tek, USA). Sagittal sections
835 of 20-25 µm thickness were made using a Leica CM3050 S cryostat, collected on
836 Superfrost Plus slides, and stored at −80°C. Multiplexed single-molecule FISH was
837 performed using the RNAscope platform (Advanced Cell Diagnostics [ACD]) according
838 to the manufacturer's protocol for fresh-frozen sections. Commercial probes obtained
839 from ACD detected the following genes: *Tnfrsf12a* (*Fn14*), *Slc17a7* (*Vglut1*), *Gad1*,
840 *Penk*, and *Chrnb3*.

841 For quantification of *Fn14*, *Slc17a7*, and *Gad1* transcripts/cell, 60X confocal images
842 were acquired using a LSM 710 Zeiss microscope. A total of 3 mice per condition and a
843 minimum of two images per mouse were analyzed. *Fn14* expression was quantified
844 using an ImageJ macro built in-house (code: www.cheadlelab.com/tools). Briefly, the
845 DAPI channel was thresholded and binarized, and subsequently expanded using the
846 dilate function. This expanded DAPI mask was then passed through a watershed filter
847 to ensure that cells that were proximal to each other were separated. This DAPI mask
848 was then used to create cell specific ROIs, where each ROI was considered a single
849 cell. Using these cell-masked ROIs, the number of FISH puncta were counted using the
850 3D image counter function within imageJ, within a given ROI. ROIs were classified with
851 the following criteria: ROIs containing 3 or more *Fn14* molecules were considered
852 positive for *Fn14*, and for markers (*GAD1* and *Vglut1*) cells were considered positive if
853 there were 5 or more marker molecules present within a given ROI.
854

855 ***Behavior***

856 *Cued Fear Conditioning*

857 On training day, subjects were placed into a square fear-conditioning arena of
858 24(w)x20(d)x30(h) cm equipped with a shock grid floor and acrylic walls patterned with
859 horizontal black and white bars 2 cm in width. Subjects were allowed to acclimate to the
860 arena for 4 minutes before data acquisition. During training, mice were presented with
861 three 20 second tones (75 dB; 2000 Hz) followed by a 2 second foot shock (0.5 mA)
862 with variable inter-trial intervals totaling 5 minutes. After training, subjects were returned
863 to their home cages for 24 hours before being tested in familiar and novel contexts. For
864 familiar context (the paired context without the cued tone; Context (-) tone) subjects
865 were re-acclimated to the test arena for 5 minutes without receiving tone cues or shocks
866 to reduce freezing to non-tone cues. After testing freezing in the Context -tone condition
867 and on the same day, subjects were exposed to a novel context (circular arena 30(w) x
868 30(h) cm, with clear acrylic floor and polka-dot walls) for 3 minutes to habituate the mice
869 to the novel context before freezing examined. Mice were then returned to their home
870 cages for 24 hours before being re-exposed to the novel context, but were then re-
871 presented with the cued tone (75 dB; 2000 Hz) for three minutes during acquisition.
872 Freezing was calculated using Ethovision XT v. 15 (Nodulus, Netherlands) where

freezing was measured using activity detection set to 300 ms and data was presented as freezing over the trial time.

Morris Water Maze

Each training trial consisted of four 90 s sub-trials in which each subject's starting position was pseudo-randomized to each of the four cardinal directions in a 137 cm wide water bath containing 24°C clear water filled up to 25 cm from the rim of the tub. The cardinal directions were marked on the wall of the tub with 20 cm diameter symbols. Subjects were initially trained over two trials where the goal zone was visible (visible trials), where the goal platform was raised 0.5 cm above the water line and was marked with a bright flag for increased visibility. Each trial ended either after the trial time expired, or after the subject correctly found and stayed on the goal platform for more than 5 seconds. If a mouse did not find the platform within 90 seconds, it was gently moved to the platform and left there for 5 seconds. The day following visible platform training, the goal platform was submerged (0.5 cm below the water line) and moved to a different quadrant. Subjects were tested on the hidden platform over 5 consecutive trials spanning 48 hours. On the fourth day (probe trial) the goal platform was removed from the testing arena and subjects were placed facing the wall opposite of the previous goal platform's position. Subjects were allowed to swim for a total of 60 s before being removed from the arena. On reversal trials (4 trials), the goal platform remained submerged, but was moved to the opposite end of the arena. Subjects started the reverse trials facing the furthest wall and were allowed to search for the goal platform for 90 s. If the subject failed to find the goal platform, the subject was oriented in the correct direction and guided to the goal platform before being removed from the arena. Latency to goal platform, distance swam, and subject position was collected using Ethovision XT v. 15 (Nodulus, Netherlands*)*.

EEG recordings and PTZ seizure induction

EEG telemetry unit implantation

Mice were implanted with wireless telemetry units (PhysioTel ETA-F10; DSI, Data Sciences International) under sterile techniques per laboratory protocol as previously described. Under anesthesia, a transmitter was placed intraperitoneally, and electrodes were threaded subcutaneously to the cranium. After skull exposure, haemostasis, and identification of the cranial sutures bregma and lambda, two 1-mm diameter burr holes were drilled over the right olfactory bulb (reference) and left occipital cortex (active). The epidural electrodes of the telemetry units, connected to the leads of the transmitter, were placed into the burr holes, and secured using stainless steel skull screws. Once in place, the skull screws were covered with dental cement. Mice were subcutaneously injected 0 and 24 hours post-operatively with 5 mg/kg meloxicam for analgesia. After 1 week of recovery, mice were individually housed in their home cages in a 12-h light–12 h dark, temperature and humidity-controlled chamber with *ad libitum* access to food and water.

913 *Baseline and PTZ seizure induction*

914 After a 24-h acclimation period, one-channel EEG was recorded differentially between
915 the reference (right olfactory bulb) and active (left occipital lobe) electrodes using the
916 Ponemah acquisition platform (DSI). EEG, core-body temperature, and locomotor
917 activity signals were continuously sampled from all mice for 48 h along with time-
918 registered videos. At the end of baseline acquisition, all mice were provoked with a
919 convulsive dose (60 mg/kg; i.p.) of the $GABA_a$ receptor antagonist pentylenetetrazole
920 (PTZ; Sigma-Aldrich, Co.) to measure seizure susceptibility and evaluate seizure
921 thresholds (Dhamne et al., 2017; Yuskaitis et al., 2018; Zullo et al., 2019). Mice were
922 continuously monitored for clinical and electrographic seizure activity for 20 minutes.

923 *Data analysis*

924 All data were processed and analyzed using Neuroscore software (DSI). Baseline EEG
925 was analyzed for spontaneous seizure activity, circadian biometrics, and spectral power
926 band analysis (Dhamne et al., 2017; Yuskaitis et al., 2018). Relative spectral power in
927 delta (1-4 Hz), theta (4-8 Hz), alpha (8-12 Hz), beta (12-30 Hz), low gamma (30-60 Hz)
928 and high gamma (60-90 Hz) frequency bands of the baseline EEG were calculated
929 using the fast Fourier transform (FFT) technique.

930 PTZ-induced seizure activity was broadly scored on a modified Raccine's scale as only
931 electrographic spikes (score: 1), myoclonic seizures (score: 3), generalized tonic-clonic
932 seizures (GTC; score: 5) and death (score: 6). Per mouse, number of myoclonic
933 seizures, latency and incidence of GTC seizures, number of GTCs, and total duration of
934 GTC were recorded. Mice without seizures were assigned a time of 20 min at the end of
935 the PTZ challenge observation period.

936 ***Blinding***

937 Experimenters were blinded to conditions at all stages of analysis. For
938 immunofluorescence, FISH, Golgi staining, and snRNAseq, one experimenter harvested
939 the tissue and assigned it a randomized label before providing the blinded tissue to
940 another experimenter for analysis. After data acquisition and processing, the data were
941 plotted in Graphpad by L.C. or A.F. after which the samples were unblinded. Similar
942 approaches were used for the behavioral and EEG experiments.

943 **References**:

944 Alver, B.H., Kim, K.H., Lu, P., Wang, X., Manchester, H.E., Wang, W., Haswell, J.R.,
945 Park, P.J., and Roberts, C.W. (2017). The SWI/SNF chromatin remodelling complex is
946 required for maintenance of lineage specific enhancers. Nat Commun *8*, 14648.
947 Badimon, A., Strasburger, H.J., Ayata, P., Chen, X., Nair, A., Ikegami, A., Hwang, P.,
948 Chan, A.T., Graves, S.M., Uweru, J.O.*, et al.* (2020). Negative feedback control of
949 neuronal activity by microglia. Nature *586*, 417-423.
950 Bannister, A.J., and Kouzarides, T. (2011). Regulation of chromatin by histone
951 modifications. Cell Res *21*, 381-395.

952 Bogershausen, N., and Wollnik, B. (2018). Mutational Landscapes and Phenotypic
953 Spectrum of SWI/SNF-Related Intellectual Disability Disorders. Front Mol Neurosci *11*,
954 252.
955 Brown, S.A., Cheng, E., Williams, M.S., and Winkles, J.A. (2013). TWEAK-independent
956 Fn14 self-association and NF-kappaB activation is mediated by the C-terminal region of
957 the Fn14 cytoplasmic domain. PLoS One *8*, e65248.
958 Brown, S.A., Richards, C.M., Hanscom, H.N., Feng, S.L., and Winkles, J.A. (2003). The
959 Fn14 cytoplasmic tail binds tumour-necrosis-factor-receptor-associated factors 1, 2, 3
960 and 5 and mediates nuclear factor-kappaB activation. Biochem J *371*, 395-403.
961 Bryk, M., Briggs, S.D., Strahl, B.D., Curcio, M.J., Allis, C.D., and Winston, F. (2002).
962 Evidence that Set1, a factor required for methylation of histone H3, regulates rDNA
963 silencing in S. cerevisiae by a Sir2-independent mechanism. Curr Biol *12*, 165-170.
964 Burkly, L.C. (2014). TWEAK/Fn14 axis: the current paradigm of tissue injury-inducible
965 function in the midst of complexities. Semin Immunol *26*, 229-236.
966 Cheadle, L., Rivera, S.A., Phelps, J.S., Ennis, K.A., Stevens, B., Burkly, L.C., Lee,
967 W.A., and Greenberg, M.E. (2020). Sensory Experience Engages Microglia to Shape
968 Neural Connectivity through a Non-Phagocytic Mechanism. Neuron *108*, 451-468 e459.
969 Cheadle, L., Tzeng, C.P., Kalish, B.T., Harmin, D.A., Rivera, S., Ling, E., Nagy, M.A.,
970 Hrvatin, S., Hu, L., Stroud, H.*, et al.* (2018). Visual Experience-Dependent Expression of
971 Fn14 Is Required for Retinogeniculate Refinement. Neuron *99*, 525-539 e510.
972 Dhamne, S.C., Silverman, J.L., Super, C.E., Lammers, S.H.T., Hameed, M.Q., Modi,
973 M.E., Copping, N.A., Pride, M.C., Smith, D.G., Rotenberg, A.*, et al.* (2017). Replicable
974 in vivo physiological and behavioral phenotypes of the Shank3B null mutant mouse
975 model of autism. Mol Autism *8*, 26.
976 Dogra, C., Hall, S.L., Wedhas, N., Linkhart, T.A., and Kumar, A. (2007). Fibroblast
977 growth factor inducible 14 (Fn14) is required for the expression of myogenic regulatory
978 factors and differentiation of myoblasts into myotubes. Evidence for TWEAK-
979 independent functions of Fn14 during myogenesis. J Biol Chem *282*, 15000-15010.
980 Dohi, T., Borodovsky, A., Wu, P., Shearstone, J.R., Kawashima, R., Runkel, L., Rajman,
981 L., Dong, X., Scott, M.L., Michaelson, J.S.*, et al.* (2009). TWEAK/Fn14 pathway: a
982 nonredundant role in intestinal damage in mice through a TWEAK/intestinal epithelial
983 cell axis. Gastroenterology *136*, 912-923.
984 Feinberg, I. (1982). Schizophrenia: caused by a fault in programmed synaptic
985 elimination during adolescence? J Psychiatr Res *17*, 319-334.
986 Ferro, A., Auguste, Y.S.S., and Cheadle, L. (2021). Microglia, Cytokines, and Neural
987 Activity: Unexpected Interactions in Brain Development and Function. Front Immunol
988 *12*, 703527.
989 Gunner, G., Cheadle, L., Johnson, K.M., Ayata, P., Badimon, A., Mondo, E., Nagy,
990 M.A., Liu, L., Bemiller, S.M., Kim, K.W.*, et al.* (2019). Sensory lesioning induces
991 microglial synapse elimination via ADAM10 and fractalkine signaling. Nat Neurosci *22*,
992 1075-1088.
993 Hammond, T.R., Marsh, S.E., and Stevens, B. (2019). Immune Signaling in
994 Neurodegeneration. Immunity *50*, 955-974.
995 Hatch, H.A.M., Belalcazar, H.M., Marshall, O.J., and Secombe, J. (2021). A KDM5-
996 Prospero transcriptional axis functions during early neurodevelopment to regulate
997 mushroom body formation. Elife *10*.

998 Hong, S., Beja-Glasser, V.F., Nfonoyim, B.M., Frouin, A., Li, S., Ramakrishnan, S.,
999 Merry, K.M., Shi, Q., Rosenthal, A., Barres, B.A.*, et al.* (2016). Complement and
1000 microglia mediate early synapse loss in Alzheimer mouse models. Science *352*, 712-
1001 716.
1002 Hong, Y.K., and Chen, C. (2011). Wiring and rewiring of the retinogeniculate synapse.
1003 Curr Opin Neurobiol *21*, 228-237.
1004 Hooks, B.M., and Chen, C. (2006). Distinct roles for spontaneous and visual activity in
1005 remodeling of the retinogeniculate synapse. Neuron *52*, 281-291.
1006 Hooks, B.M., and Chen, C. (2008). Vision triggers an experience-dependent sensitive
1007 period at the retinogeniculate synapse. J Neurosci *28*, 4807-4817.
1008 Hooks, B.M., and Chen, C. (2020). Circuitry Underlying Experience-Dependent
1009 Plasticity in the Mouse Visual System. Neuron *106*, 21-36.
1010 Hyun, K., Jeon, J., Park, K., and Kim, J. (2017). Writing, erasing and reading histone
1011 lysine methylations. Exp Mol Med *49*, e324.
1012 Jakubowski, A., Ambrose, C., Parr, M., Lincecum, J.M., Wang, M.Z., Zheng, T.S.,
1013 Browning, B., Michaelson, J.S., Baetscher, M., Wang, B.*, et al.* (2005). TWEAK induces
1014 liver progenitor cell proliferation. J Clin Invest *115*, 2330-2340.
1015 Kakegawa, W., Mitakidis, N., Miura, E., Abe, M., Matsuda, K., Takeo, Y.H., Kohda, K.,
1016 Motohashi, J., Takahashi, A., Nagao, S.*, et al.* (2015). Anterograde C1ql1 signaling is
1017 required in order to determine and maintain a single-winner climbing fiber in the mouse
1018 cerebellum. Neuron *85*, 316-329.
1019 Kalish, B.T., Cheadle, L., Hrvatin, S., Nagy, M.A., Rivera, S., Crow, M., Gillis, J.,
1020 Kirchner, R., and Greenberg, M.E. (2018). Single-cell transcriptomics of the developing
1021 lateral geniculate nucleus reveals insights into circuit assembly and refinement. Proc
1022 Natl Acad Sci U S A *115*, E1051-E1060.
1023 Kim, J., Kim, J.A., McGinty, R.K., Nguyen, U.T., Muir, T.W., Allis, C.D., and Roeder,
1024 R.G. (2013). The n-SET domain of Set1 regulates H2B ubiquitylation-dependent H3K4
1025 methylation. Mol Cell *49*, 1121-1133.
1026 LeBlanc, J.J., and Fagiolini, M. (2011). Autism: a "critical period" disorder? Neural Plast
1027 *2011*, 921680.
1028 Li, M., Li, Z., Ren, H., Jin, W.N., Wood, K., Liu, Q., Sheth, K.N., and Shi, F.D. (2017).
1029 Colony stimulating factor 1 receptor inhibition eliminates microglia and attenuates brain
1030 injury after intracerebral hemorrhage. J Cereb Blood Flow Metab *37*, 2383-2395.
1031 Macosko, E.Z., Basu, A., Satija, R., Nemesh, J., Shekhar, K., Goldman, M., Tirosh, I.,
1032 Bialas, A.R., Kamitaki, N., Martersteck, E.M.*, et al.* (2015). Highly Parallel Genome-wide
1033 Expression Profiling of Individual Cells Using Nanoliter Droplets. Cell *161*, 1202-1214.
1034 McGinnis, C.S., Murrow, L.M., and Gartner, Z.J. (2019). DoubletFinder: Doublet
1035 Detection in Single-Cell RNA Sequencing Data Using Artificial Nearest Neighbors. Cell
1036 Syst *8*, 329-337 e324.
1037 Meighan-Mantha, R.L., Hsu, D.K., Guo, Y., Brown, S.A., Feng, S.L., Peifley, K.A.,
1038 Alberts, G.F., Copeland, N.G., Gilbert, D.J., Jenkins, N.A.*, et al.* (1999). The mitogen-
1039 inducible Fn14 gene encodes a type I transmembrane protein that modulates fibroblast
1040 adhesion and migration. J Biol Chem *274*, 33166-33176.
1041 Mi, H., Muruganujan, A., Casagrande, J.T., and Thomas, P.D. (2013). Large-scale gene
1042 function analysis with the PANTHER classification system. Nat Protoc *8*, 1551-1566.

1043 Miyamoto, A., Wake, H., Ishikawa, A.W., Eto, K., Shibata, K., Murakoshi, H., Koizumi,
1044 S., Moorhouse, A.J., Yoshimura, Y., and Nabekura, J. (2016). Microglia contact induces
1045 synapse formation in developing somatosensory cortex. Nat Commun *7*, 12540.
1046 Nagy, D., Ennis, K.A., Wei, R., Su, S.C., Hinckley, C.A., Gu, R.F., Gao, B., Massol,
1047 R.H., Ehrenfels, C., Jandreski, L.*, et al.* (2021). Developmental synaptic regulator,
1048 TWEAK/Fn14 signaling, is a determinant of synaptic function in models of stroke and
1049 neurodegeneration. Proc Natl Acad Sci U S A *118*.
1050 Nguyen, P.T., Dorman, L.C., Pan, S., Vainchtein, I.D., Han, R.T., Nakao-Inoue, H.,
1051 Taloma, S.E., Barron, J.J., Molofsky, A.B., Kheirbek, M.A.*, et al.* (2020). Microglial
1052 Remodeling of the Extracellular Matrix Promotes Synapse Plasticity. Cell *182*, 388-403
1053 e315.
1054 Paolicelli, R.C., Bolasco, G., Pagani, F., Maggi, L., Scianni, M., Panzanelli, P.,
1055 Giustetto, M., Ferreira, T.A., Guiducci, E., Dumas, L.*, et al.* (2011). Synaptic pruning by
1056 microglia is necessary for normal brain development. Science *333*, 1456-1458.
1057 Paolicelli, R.C., and Gross, C.T. (2011). Microglia in development: linking brain wiring to
1058 brain environment. Neuron Glia Biol *7*, 77-83.
1059 Park, S.Y., and Kim, J.S. (2020). A short guide to histone deacetylases including recent
1060 progress on class II enzymes. Exp Mol Med *52*, 204-212.
1061 Pelkey, K.A., Chittajallu, R., Craig, M.T., Tricoire, L., Wester, J.C., and McBain, C.J.
1062 (2017). Hippocampal GABAergic Inhibitory Interneurons. Physiol Rev *97*, 1619-1747.
1063 Perrault, I., Hamdan, F.F., Rio, M., Capo-Chichi, J.M., Boddaert, N., Decarie, J.C.,
1064 Maranda, B., Nabbout, R., Sylvain, M., Lortie, A.*, et al.* (2014). Mutations in DOCK7 in
1065 individuals with epileptic encephalopathy and cortical blindness. Am J Hum Genet *94*,
1066 891-897.
1067 Qiu, X., Mao, Q., Tang, Y., Wang, L., Chawla, R., Pliner, H.A., and Trapnell, C. (2017).
1068 Reversed graph embedding resolves complex single-cell trajectories. Nat Methods.
1069 Schafer, D.P., Lehrman, E.K., Kautzman, A.G., Koyama, R., Mardinly, A.R., Yamasaki,
1070 R., Ransohoff, R.M., Greenberg, M.E., Barres, B.A., and Stevens, B. (2012). Microglia
1071 sculpt postnatal neural circuits in an activity and complement-dependent manner.
1072 Neuron *74*, 691-705.
1073 Shen, E., Shulha, H., Weng, Z., and Akbarian, S. (2014). Regulation of histone H3K4
1074 methylation in brain development and disease. Philos Trans R Soc Lond B Biol Sci *369*.
1075 Sokpor, G., Xie, Y., Rosenbusch, J., and Tuoc, T. (2017). Chromatin Remodeling BAF
1076 (SWI/SNF) Complexes in Neural Development and Disorders. Front Mol Neurosci *10*,
1077 243.
1078 Stevens, B., Allen, N.J., Vazquez, L.E., Howell, G.R., Christopherson, K.S., Nouri, N.,
1079 Micheva, K.D., Mehalow, A.K., Huberman, A.D., Stafford, B.*, et al.* (2007). The classical
1080 complement cascade mediates CNS synapse elimination. Cell *131*, 1164-1178.
1081 Stroud, H., Su, S.C., Hrvatin, S., Greben, A.W., Renthal, W., Boxer, L.D., Nagy, M.A.,
1082 Hochbaum, D.R., Kinde, B., Gabel, H.W.*, et al.* (2017). Early-Life Gene Expression in
1083 Neurons Modulates Lasting Epigenetic States. Cell.
1084 Stroud, H., Yang, M.G., Tsitohay, Y.N., Davis, C.P., Sherman, M.A., Hrvatin, S., Ling,
1085 E., and Greenberg, M.E. (2020). An Activity-Mediated Transition in Transcription in
1086 Early Postnatal Neurons. Neuron *107*, 874-890 e878.

1087 Stuart, T., Butler, A., Hoffman, P., Hafemeister, C., Papalexi, E., Mauck, W.M., 3rd,
1088 Hao, Y., Stoeckius, M., Smibert, P., and Satija, R. (2019). Comprehensive Integration of
1089 Single-Cell Data. Cell *177*, 1888-1902 e1821.
1090 Swahari, V., and West, A.E. (2019). Histone demethylases in neuronal differentiation,
1091 plasticity, and disease. Curr Opin Neurobiol *59*, 9-15.
1092 Tai, Y., Janas, J.A., Wang, C.L., and Van Aelst, L. (2014). Regulation of chandelier cell
1093 cartridge and bouton development via DOCK7-mediated ErbB4 activation. Cell Rep *6*,
1094 254-263.
1095 Tran, N.L., McDonough, W.S., Savitch, B.A., Fortin, S.P., Winkles, J.A., Symons, M.,
1096 Nakada, M., Cunliffe, H.E., Hostetter, G., Hoelzinger, D.B.*, et al.* (2006). Increased
1097 fibroblast growth factor-inducible 14 expression levels promote glioma cell invasion via
1098 Rac1 and nuclear factor-kappaB and correlate with poor patient outcome. Cancer Res
1099 *66*, 9535-9542.
1100 Vainchtein, I.D., Chin, G., Cho, F.S., Kelley, K.W., Miller, J.G., Chien, E.C., Liddelow,
1101 S.A., Nguyen, P.T., Nakao-Inoue, H., Dorman, L.C.*, et al.* (2018). Astrocyte-derived
1102 interleukin-33 promotes microglial synapse engulfment and neural circuit development.
1103 Science *359*, 1269-1273.
1104 Van Erum, J., Van Dam, D., and De Deyn, P.P. (2019). PTZ-induced seizures in mice
1105 require a revised Racine scale. Epilepsy Behav *95*, 51-55.
1106 Vierbuchen, T., Ling, E., Cowley, C.J., Couch, C.H., Wang, X., Harmin, D.A., Roberts,
1107 C.W.M., and Greenberg, M.E. (2017). AP-1 Transcription Factors and the BAF Complex
1108 Mediate Signal-Dependent Enhancer Selection. Mol Cell *68*, 1067-1082 e1012.
1109 Wang, C., Yue, H., Hu, Z., Shen, Y., Ma, J., Li, J., Wang, X.D., Wang, L., Sun, B., Shi,
1110 P.*, et al.* (2020). Microglia mediate forgetting via complement-dependent synaptic
1111 elimination. Science *367*, 688-694.
1112 Wiesel, T.N., and Hubel, D.H. (1963a). Effects of Visual Deprivation on Morphology and
1113 Physiology of Cells in the Cats Lateral Geniculate Body. J Neurophysiol *26*, 978-993.
1114 Wiesel, T.N., and Hubel, D.H. (1963b). Single-Cell Responses in Striate Cortex of
1115 Kittens Deprived of Vision in One Eye. J Neurophysiol *26*, 1003-1017.
1116 Wijayatunge, R., Chen, L.F., Cha, Y.M., Zannas, A.S., Frank, C.L., and West, A.E.
1117 (2014). The histone lysine demethylase Kdm6b is required for activity-dependent
1118 preconditioning of hippocampal neuronal survival. Mol Cell Neurosci *61*, 187-200.
1119 Wijayatunge, R., Liu, F., Shpargel, K.B., Wayne, N.J., Chan, U., Boua, J.V., Magnuson,
1120 T., and West, A.E. (2018). The histone demethylase Kdm6b regulates a mature gene
1121 expression program in differentiating cerebellar granule neurons. Mol Cell Neurosci *87*,
1122 4-17.
1123 Wiley, S.R., and Winkles, J.A. (2003). TWEAK, a member of the TNF superfamily, is a
1124 multifunctional cytokine that binds the TweakR/Fn14 receptor. Cytokine Growth Factor
1125 Rev *14*, 241-249.
1126 Xie, Z., Srivastava, D.P., Photowala, H., Kai, L., Cahill, M.E., Woolfrey, K.M., Shum,
1127 C.Y., Surmeier, D.J., and Penzes, P. (2007). Kalirin-7 controls activity-dependent
1128 structural and functional plasticity of dendritic spines. Neuron *56*, 640-656.
1129 Yuskaitis, C.J., Jones, B.M., Wolfson, R.L., Super, C.E., Dhamne, S.C., Rotenberg, A.,
1130 Sabatini, D.M., Sahin, M., and Poduri, A. (2018). A mouse model of DEPDC5-related
1131 epilepsy: Neuronal loss of Depdc5 causes dysplastic and ectopic neurons, increased
1132 mTOR signaling, and seizure susceptibility. Neurobiol Dis *111*, 91-101.

1133 Zilionis, R., Nainys, J., Veres, A., Savova, V., Zemmour, D., Klein, A.M., and Mazutis, L.
1134 (2017). Single-cell barcoding and sequencing using droplet microfluidics. Nat Protoc *12*,
1135 44-73.
1136 Zullo, J.M., Drake, D., Aron, L., O'Hern, P., Dhamne, S.C., Davidsohn, N., Mao, C.A.,
1137 Klein, W.H., Rotenberg, A., Bennett, D.A.*, et al.* (2019). Regulation of lifespan by neural
1138 excitation and REST. Nature *574*, 359-364.

1139

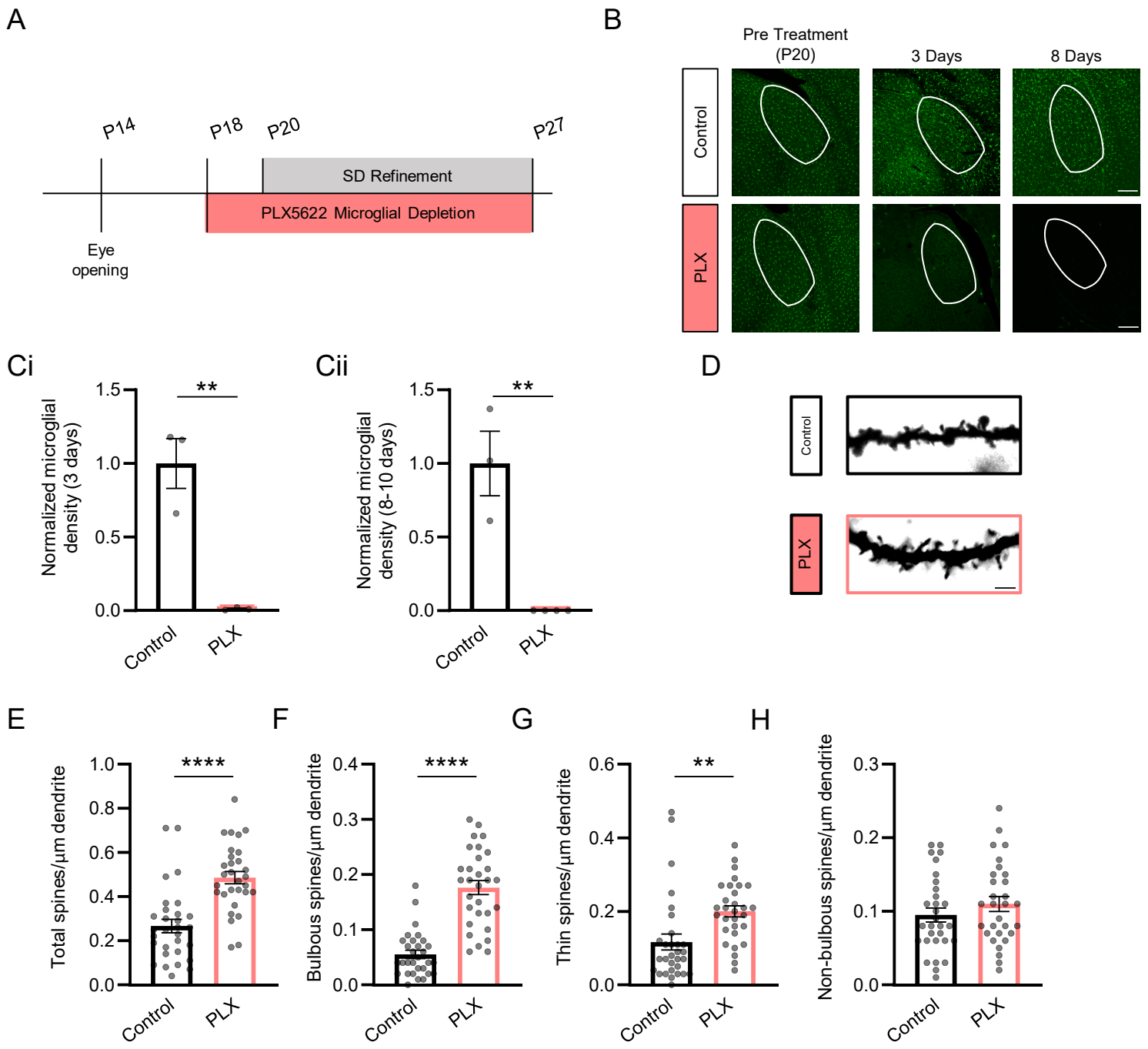

Figure 1. Microglia are required for sensory-dependent refinement in the dLGN.

Figure 1. Microglia are required for sensory-dependent refinement in the dLGN. (A) Timeline of retinogeniculate development and Plexxikon-5622 (PLX) treatment schedule. (B) Confocal images of microglia stained for Iba1 (green) in control and PLX-treated mice before PLX-administration at P20, 3 days into treatment, and 8 days into treatment (white outlines, dLGN. Scale bars, 200 μm). (C) Quantification of the number of microglia in mice fed PLX or control chow confirming near complete depletion of microglia following PLX administration for 3 (Ci) or 8 (Cii) days (n = 3 mice/group). (D) Example images of TC neuron spines from PLX and control mice. Scale bar, 2 μm. (E)-(H) Quantifications of the densities of all spines (E), bulbous spines (F), thin spines (G), and non-bulbous spines (H) between PLX and control mice. Data presented as mean ± SEM (Control: n =30, PLX: n = 30 spines from 3 mice/condition). Unpaired, 2-tailed student's T test (**$p < 0.01$, **** $p < 0.0001$).

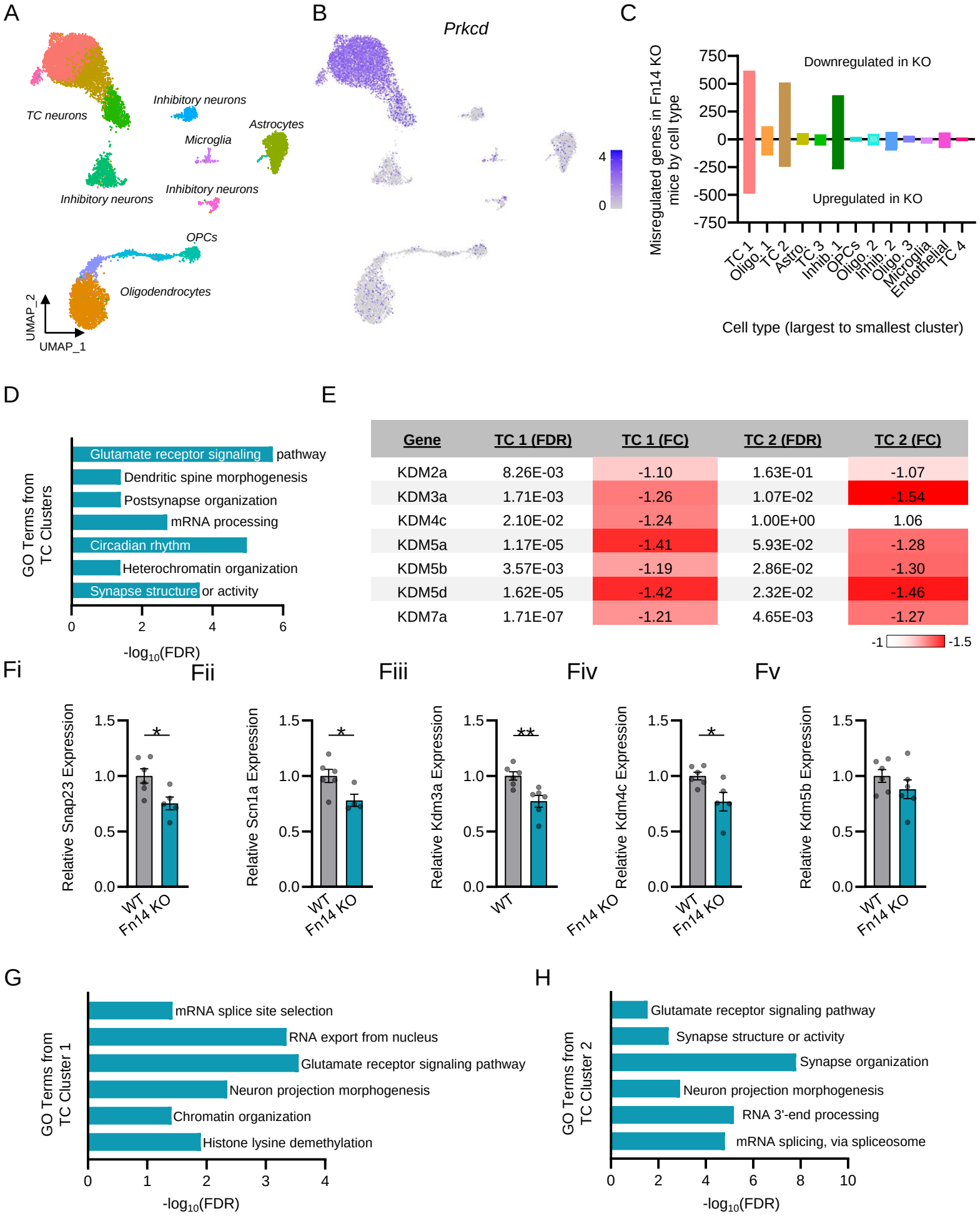

Gene	TC 1 (FDR)	TC 1 (FC)	TC 2 (FDR)	TC 2 (FC)
KDM2a	8.26E-03	-1.10	1.63E-01	-1.07
KDM3a	1.71E-03	-1.26	1.07E-02	-1.54
KDM4c	2.10E-02	-1.24	1.00E+00	1.06
KDM5a	1.17E-05	-1.41	5.93E-02	-1.28
KDM5b	3.57E-03	-1.19	2.86E-02	-1.30
KDM5d	1.62E-05	-1.42	2.32E-02	-1.46
KDM7a	1.71E-07	-1.21	4.65E-03	-1.27

Figure 2. Characterization of Fn14-regulated genes in thalamocortical (TC) neurons of the dLGN by snRNAseq.

Figure 2. Characterization of Fn14-regulated genes in thalamocortical (TC) neurons of the dLGN by snRNAseq. (A) UMAP (Uniform Manifold Approximation and Projection for Dimension Reduction) plot displaying cell clusters present in the snRNAseq dataset. (B) Selective expression of the TC neuron marker *Prkcd* in TC neuron clusters (color intensity scale: log normalized transcripts per cell). (C) Histogram displaying the numbers of differentially expressed genes (FDR < 0.05, Log2FC > |±1.25|) between Fn14 WT and KO mice. Genes downregulated in the Fn14 knockout (KO), above x-axis; genes downregulated in the KO, upregulated below x-axis. (D) Select GO (gene ontology, PANTHER terms) categories enriched in downregulated genes from both TC clusters 1 and 2 in the Fn14 KO mouse. (E) Table of histone lysine demethylases (KDMs) and the degree of their mis-regulation in the Fn14 KO mouse in TC clusters 1 and 2. (Fi-Fv) qPCR analysis of whole brain tissue validating the downregulation of select genes in Fn14 KO mice normalized to *GAPDH* expression. KO values are normalized to WT values. Data represent the mean ± SEM with individual data points representing individual mice (n = 4-6 mice/group). Unpaired, 2-tailed student's T test (*p < 0.05, **p < 0.01). (G),(H) Select significantly enriched GO terms from downregulated genes in TC clusters 1 (G) and 2, (H). respectively. Cell cluster abbreviations: Thalamocortical neurons (TC) Oligodendrocytes (Oligo.), Astrocytes (Astro.), Inhibitory neurons (Inhib.), Oligodendrocyte precursor cells (OPCs).

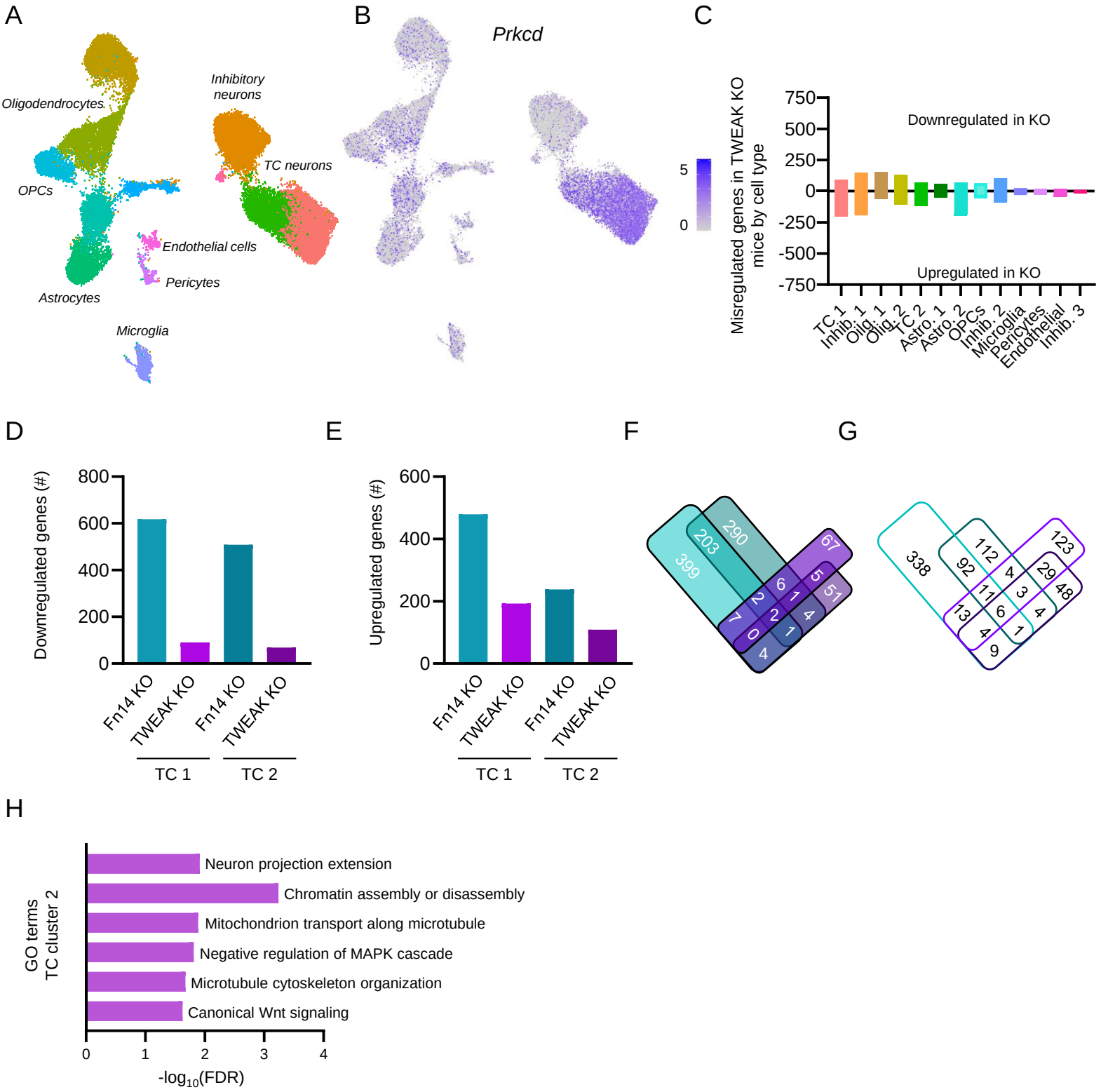

Figure 3. Characterization of TWEAK-regulated genes in thalamocortical (TC) neurons of the dLGN by snRNAseq.

Figure 3. Characterization of TWEAK-regulated genes in thalamocortical (TC) neurons of the dLGN by snRNAseq. (A) UMAP (Uniform Manifold Approximation and Projection for Dimension Reduction) plot displaying cell clusters present in the snRNAseq dataset. (B) Selective expression of the TC neuron marker *Prkcd* in TC neuron clusters (color intensity scale, log normalized transcripts per cell). (C) Histogram displaying the numbers of differentially expressed genes (FDR < 0.05, Log2FC > |±1.25|) between TWEAK WT and knockout (KO) mice. Genes downregulated in the KO, above x-axis; genes upregulated in the KO, below x-axis. Y-axis scaled for comparison with graph in Fig. 2C. (D) Comparison of the numbers of genes significantly downregulated in Fn14 and TWEAK KO mice, TC clusters 1 and 2. (E) Comparison of the numbers of genes significantly upregulated in Fn14 and TWEAK KO mice, TC clusters 1 and 2. (F) Venn diagram displaying limited overlap between differentially expressed genes in TWEAK and Fn14 KO mice for genes that are downregulated in the respective KOs. (G) Venn diagram displaying limited overlap between differentially expressed genes in TWEAK and Fn14 KO mice for genes that are upregulated in the respective KOs. (H) Select significantly enriched GO terms from downregulated genes in TWEAK KO cluster 2. Cell cluster abbreviations: Thalamocortical neurons (TC) Oligodendrocytes (Oligo.), Astrocytes (Astro.), Inhibitory neurons (Inhib.), Oligodendrocyte precursor cells (OPCs), Endothelial cells (Endo.).

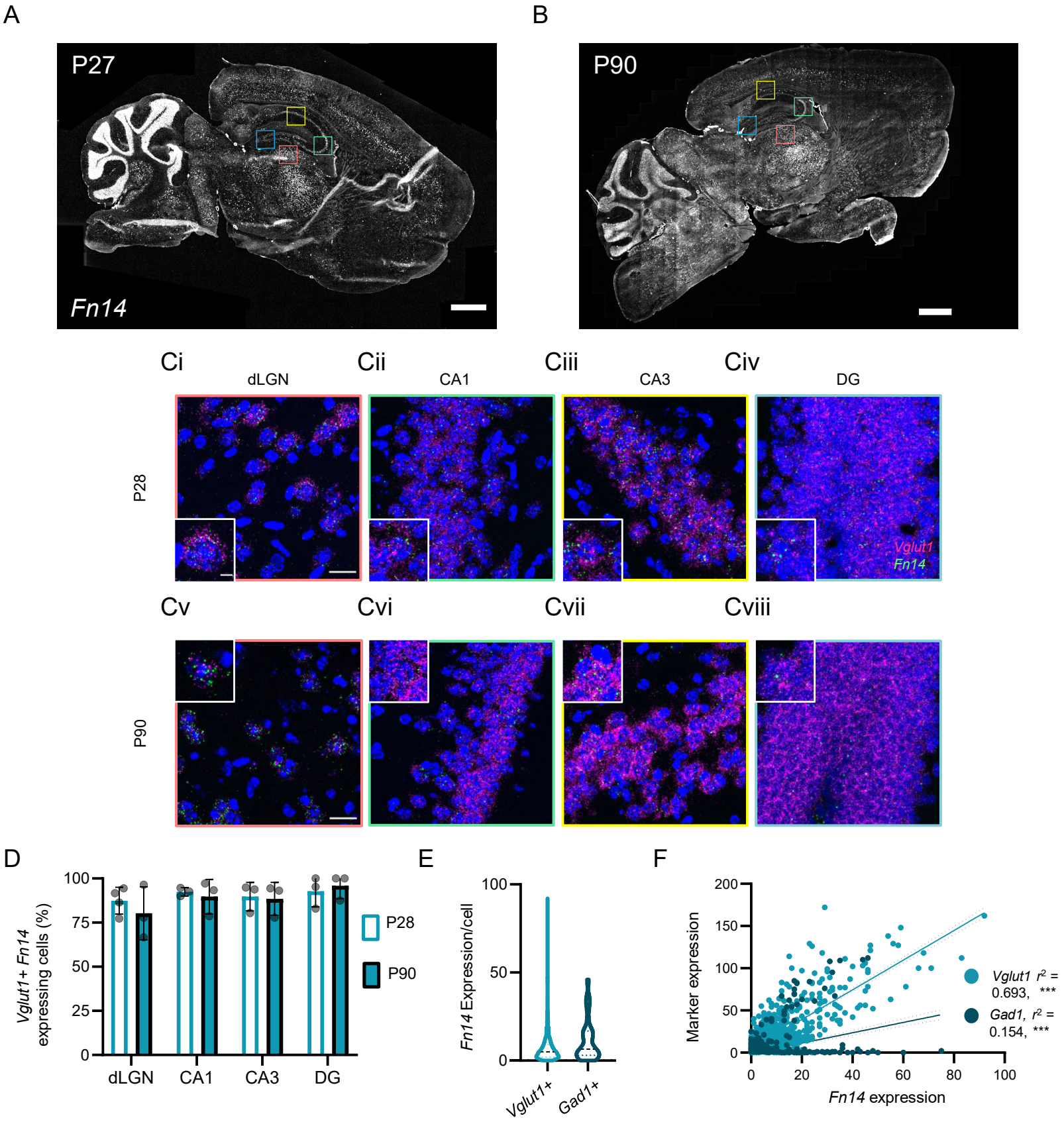

Figure 4. Whole-brain analysis of Fn14 expression during development and in the adult.

Figure 4. Whole-brain analysis of Fn14 expression during development and in the adult. (A) Sagittal scan of Fn14 expression (white) in the brain at P28. Boxes correspond with subregions of the hippocampus displayed in 3C. Scale bar, 1 mm. (B) Sagittal scan of Fn14 expression (white) in the brain at P90. Scale bar, 1 mm. (C) High-resolution (63x) confocal images of dLGN (Ci,v), CA1 (Cii,vi), CA3 (Ciii,vii) and dentate gyrus (Civ,Cviii). P28, top row. P90, bottom row. *Fn14* (green), *Vglut1* (magenta), DAPI (blue). Scale bars, 20 µm, and 5 µm for insets. (D) Quantification of the percentage of *Fn14*+ cells that are *Vglut1*+ excitatory neurons. 89.3% of *Fn14*+ cells are also *Vglut1*+ across brain regions and timepoints. (E) Amount of Fn14 in excitatory (*Vglut1*+) and inhibitory (*Gad1*+) neurons that express *Fn14* across ages. Violin plot of *Fn14* puncta/*Vglut1*+ (n = 1178 cells) or *Gad1*+ cells (n = 72 cells) ($p > 0.05$, Mann-Whitney). (F) Correlations between *Fn14* expression (x-axis) and marker gene expression (y-axis) reveals that *Fn14* expression is most closely correlated with *Vglut1* expression. Slope and R^2 values given in graph, and slopes were compared with linear regression analysis. Dotted lines represent each linear regressions' confidence (95% confidence intervals).

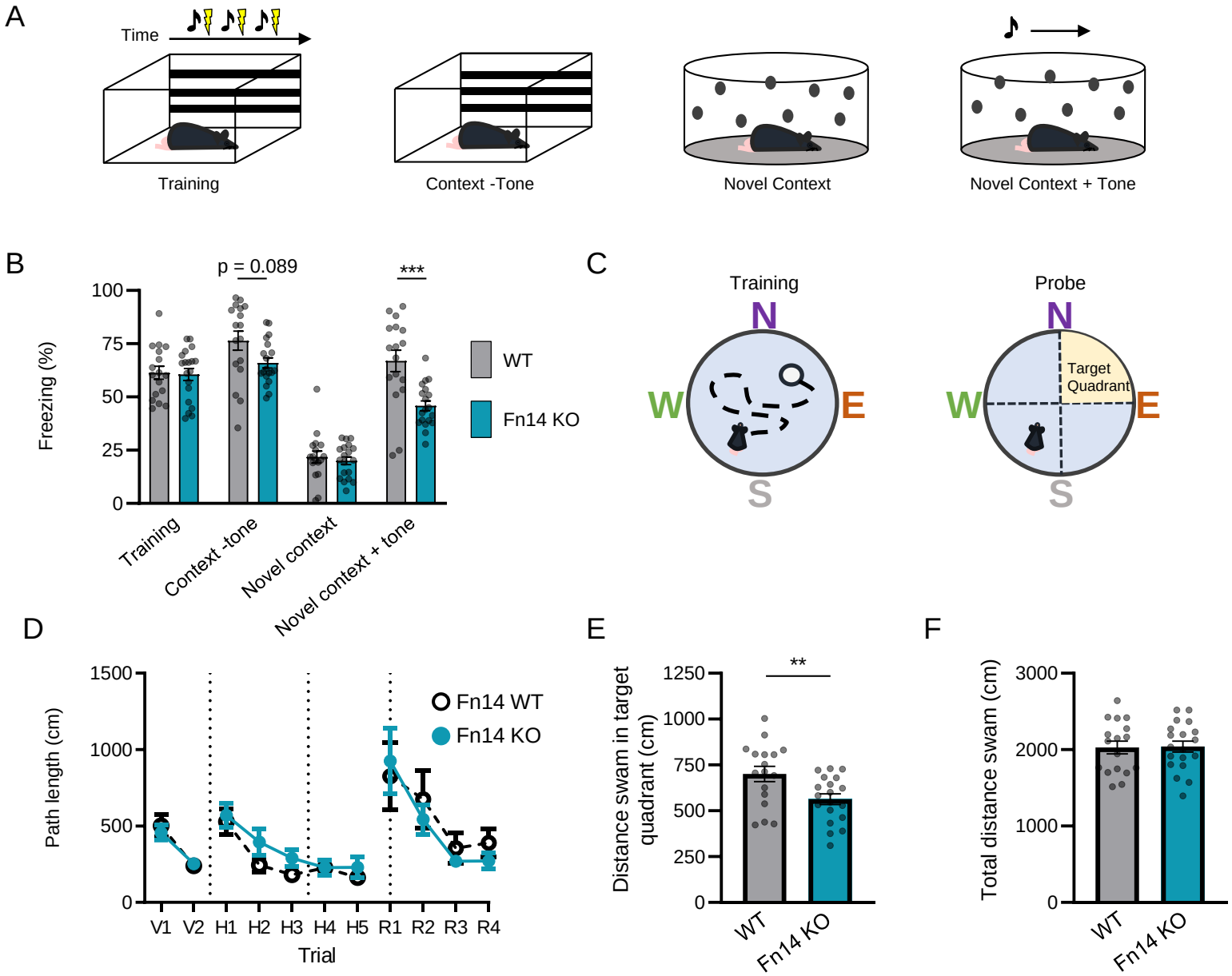

Figure 5. Loss of Fn14 impairs memory but not learning in multiple behavioral tasks.

Figure 5. **Loss of Fn14 impairs memory but not learning in multiple behavioral tasks.** (A) Diagram of cued fear conditioning (CFC) paradigm. Mice are initially conditioned to a foot shock associated with both a novel striped arena (i.e. context) and an audible tone. Mice are then re-introduced into the same context and freezing is quantified as a measure of their ability to remember the association of the context with the foot shock. Mice are then placed in an entirely novel arena without a tone and, after 24 hours, mice are placed into the novel context and are re-presented with the tone. (B) Quantifications of percentage of time spent freezing across all conditions (repeated measures ANOVA, trial: $p < 0.0001$; genotype: $p < 0.05$; subject, trial x genotype: $p < 0.0001$). Bonferroni corrected multiple comparisons WT versus KO for Context (-) tone: $p = 0.089$; Novel context + tone: $p < 0.001$. (C) Diagram of Morris Water Maze (MWM) training and probe trials. (D) Distance swam during training (repeated measures ANOVA with Šídák's multiple comparisons test: Visible; genotype: $p > 0.05$, trial: $p < 0.0001$, trial x genotype: $p > 0.05$, Hidden; genotype: $p > 0.05$, trial: $p < 0.0001$, trial x genotype: $p > 0.05$, Reverse; genotype: $p > 0.05$, trial: $p < 0.001$, trial x genotype: $p > 0.05$). (E) Distance swam in the target quadrant during probe trials. (F) Total distance swam during probe trail. Data presented as mean ± S.E.M. with data points representing individual mice. (E) and (F) Analyzed with student's T test (*$p < 0.05$, **$p < 0.01$, ***$p < 0.001$).

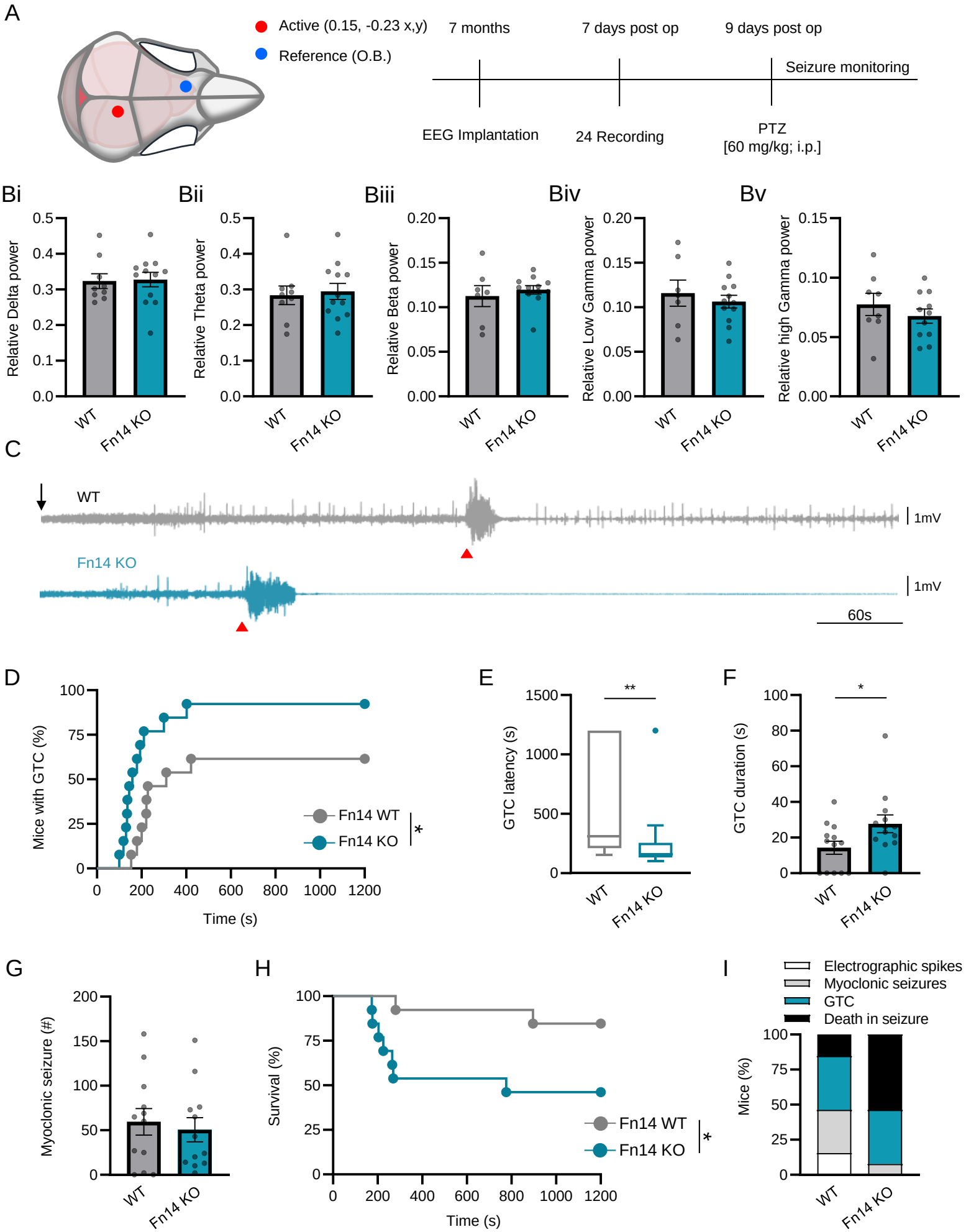

Figure 6. Loss of Fn14 confers seizure susceptibility and increased mortality following exposure to PTZ

Figure 6. Loss of Fn14 confers seizure susceptibility and increased mortality following exposure to PTZ. (A) Schematic of electroencephalogram (EEG) electrode placement and the experimental timeline. (B) Averaged EEG spectral power across frequency bands were equal between Fn14 knockout (KO) and WT mice (WT n = 11, Fn14 KO n = 12, unpaired Student's t-test $p > 0.05$). (C) Example EEG traces from WT (gray) and Fn14 KO (blue) mice after PTZ injection (black arrow). Red triangles indicate the onset of general tonic clonic (GTC) seizures (WT: latency = 311 s, duration = 19.8 s; Fn14 KO: latency = 159 s, duration = 35 s). The Fn14 KO mouse died shortly after the GTC, demonstrated by the elimination of signal following the seizure. (D) Percentage of mice that had GTC seizures relative to the time course of the experiment (WT; n = 13 median = 311 s, Fn14 KO; n = 13, median = 159 s; Log-Rank test). (E) Latency between PTZ injection and GTC onset (Mann-Whitney). (F) Duration of GTCs (unpaired Student's T-test). (G) Number of PTZ-induced myoclonic seizures (Mann-Whitney, $p > 0.05$). (H) Mortality rate of Fn14 KO and WT mice following PTZ administration. (I) The fraction of mice presenting with electrophysiological spikes (white), myoclonic seizures (grey), GTCs (teal), or death as their worst PTZ-induced outcome.